The Fresnel Interferometric Imager

Laurent Koechlin, (P.I.)
Denis Serre,
Paul Deba,
Truswin Raksasataya,
Christelle Peillon
Equipe Signal Image & Instrumentation
Laboratoire d'Astrophysique de Toulouse-Tarbes
Observatoire Midi-Pyrénées (OMP)
UMR 5572 - Signal Image & Instrumentation
14 avenue Edouard Belin
31400 Toulouse, FRANCE

Francois Bouchy,
Jean-Michel Desert,
David Ehrenreich,
Guillaume Hebrard,
Alain Lecavelier des Etangs,
Roger Ferlet,
David Sing,
Alfred Vidal-Madjar. (co I.)
Institut d'Astrophysique de Paris (IAP)
UMR7095 CNRS, Universite Pierre & Marie Curie,
98 bis boulevard Arago,
75014 Paris, FRANCE

Ana Ines Gomez de Castro (co I.)
Fac. de CC Matematicas
Universidad Complutense de Madrid
28040 Madrid, SPAIN

Roser Peillo
Equipe Physique des Galaxies
Laboratoire d'Astrophysique de Toulouse-Tarbes
Observatoire Midi-Pyrénées (OMP)
UMR 5572 - Signal Image & Instrumentation
14 avenue Edouard Belin
31400 Toulouse, FRANCE

Margarita Karovska (co I.)
Harvard Smithsonian Center for Astrophysics (CfA)
60 Garden St.
Cambridge Ma 02138, USA

Paul Duchon,
Pierre-Yves Guidotti *(stage 2004)*
Centre National d'Etudes Spatiales (CNES)
18 avenue Edouard Belin
31400 Toulouse, FRANCE

The Fresnel Interferometric Imager

I Executive Summary

I.1 Goals

The Fresnel Interferometric Imager is a class L mission that addresses several themes of the Cosmic Vision Plan : Exoplanet study, matter in extreme conditions, and the Universe taking shape. The proposed instrument is basically a general-purpose lightweight telescope, but using a novel optical concept based on interferometry, which yields high angular resolution, high dynamic range, and field, while releasing constraints on positioning and manufacturing of the optically active elements.

I.2 Principle

In this two spacecraft formation-flying mission, the main spacecraft is the focussing element : the Fresnel interferometric array ; the other spacecraft holds the field optics and detectors.

The Fresnel array is a 3.6 x 3.6 meter square opaque foil with 10^5 to 10^6 void subapertures. Focusing is achieved with no optical element : the shape and positioning of the subapertures being responsible for beam combining by diffraction for a fraction (5 to 10%) of the incident light. The consequence of this high number of subapertures is high dynamic range imaging. In addition, it is potentially efficient over a very broad wavelength domain.

This interferometric array can be seen either as an aperture synthesis array or as a particular case of diffractive zone plate. Beams from the individual subapertures are recombined by diffraction and interference. The subapertures are positioned so that a 2-π phase shift occurs at the first order of diffraction between neighboring zones. As a consequence of the subaperture positioning law, an incoming plane-wave is turned into a spherical outgoing wavefront. An image is directly formed by the array, the dense subaperture layout leading to a compact and highly contrasted Point Spread Function (PSF).

Fresnel interferometric arrays differ on several aspects from zone plates. Their layout makes the non-transmissive zones connected throughout the array, allowing the use of vacuum for the transmissive zones (subapertures) while preserving mechanical cohesion of the whole frame.

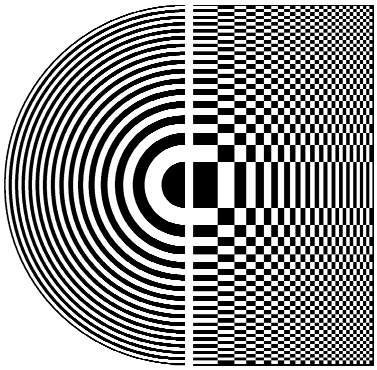

Fig I-1: Circular (Soret) zone plate & example of orthogonal Fresnel array, 15 Fresnel zones (half sides).

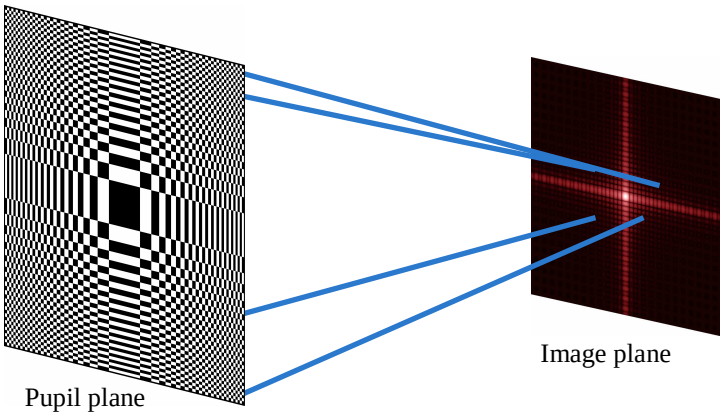

FigI-2: Image of a point source (Point Spread Function computed by Fresnel Transform).

I.3 Features, pros and cons

– As for an interferometric array, the angular resolution of a Fresnel array is the same as that of a filled aperture having the size of the whole array. The large number of subapertures provides an advantage in field.

– The use of vacuum for the individual subapertures eliminates phase defects and spectral limitations, which would result from the use of a transparent or reflective material. The spectral span of Fresnel arrays is bounded by the characteristics of the opaque foil : towards the UV by its effective opacity, towards the I.R. by its Plank emission. A spectral domain spanning from 100 nanometers to 10 microns is expected.

– The resulting wavefront quality is restricted by the precision with which subapertures are carved. This constraint is loose compared to optical surfacing : a λ/50 quality wavefront (required for high dynamic range imaging) is obtained with either a λ/100 mirror (5 nanometer precision for the visible), or a 0.1 millimeter precision subaperture positioning in the plane of the Fresnel array. The required precision in the perpendicular (propagation) direction is in the order of a centimeter. The precision to which subapertures in a Fresnel array have to be

positioned is not wavelength dependant.

– The pattern of the array : all subaperture edges following two orthogonal (or close to orthogonal) directions, casts light at focus into a central peak flanked by two orthogonal spikes, rather than the diffraction rings occurring with circular apertures, or broad side lobes (case of diluted interferometric arrays). Most of the image field of a Fresnel array is at very high rejection rate. To further increase the dynamic range, apodization is used, either by modulating the size of subapertures from center to limb of the array, else at a smaller pupil plane with "Phase Induced Amplitude Apodization" dedicated optics.

– The very large number of subapertures allows a high field/resolution ratio, hence much wider fields than other interferometers : a simple law relates the achievable field of an interferometer to the number of subapertures it includes.

– Fresnel arrays act as transmission gratings. Half of the incoming light is blocked by the opaque foil, a major part of the transmitted remains a plane wave, so only 5 to 10% of the light is focused, this proportion depending on the subaperture optimization and positioning. As a consequence, a 3 to 4-fold increase in size is required to collect the same number of photons as a solid aperture. The comparison in terms of image brightness depends if the object is extended or unresolved. In all cases, if comparison with filled apertures is made in terms of cost rather than size, per photon or per valuable datum, Fresnel arrays should get the advantage.

– Strong chromatism occurs as a consequence of diffractive focussing at order +1: $f \propto 1/\lambda$. This chromatism is cancelled by a small diffractive element in the focal instrumentation, operating at diffraction order -1. This secondary Fresnel lens is blazed to optimize transmission. The resulting correction is complete and independent of the wavelength. However, for a given inter-spacecraft distance, the bandwidth is limited to $\Delta\lambda/\lambda = 20\%$ due to the size of the field optics in the secondary spacecraft. With six adjustable wavelength channels side by side, we propose to cover regions of interest in the U.V ; Visible and I.R domains. Light will be fed into one channel at a time by changing the attitude of the secondary spacecraft, and the inter-spacecraft distance adjusted accordingly.

– Long focal lengths are implied. For example 2.5 to 18 km for a 3.6-meter array operated at respectively $\lambda \approx 1$ µm and $\lambda \approx 100$nm, therefore requiring formation flying in a low gravity gradient region of space.

I.4 State of the art

We propose a 3.6 meter Fresnel interferometric array; the concept has been tested for now three years : we have built a 22-meter focal length breadboard design and tested it at Observatoire Midi-Pyrénées (Toulouse, France).

Fig I-3: 80 mm square Fresnel primary array carved into a thin 80 µm stainless steel foil, used for optical tests. (58 Fresnel zones, 26 680 subapertures).

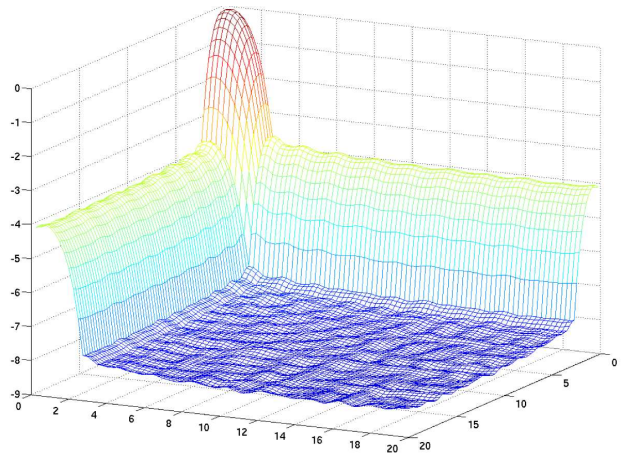

Fig 1-4: Simulated quarter field PSF of an apodized 300 zone Fresnel array. Vertical axis : log normalized brightness. Horizontal plane: position in the field, in units of diffraction limited resolution radius (resel).

We have tested the efficiency of the chromatism correction on artificial sources, (500nm < λ < 750nm), the image quality (diffraction limited) and the dynamic range. At present, the highest dynamic range of a detected double source is $6.2\ 10^{-6}$ with this optical prototype. It has also allowed to validate numerical simulation algorithms for larger Fresnel interferometric arrays. These simulations yield a dynamic range (rejection factor) close to 10^{-8} for arrays such as the 3.6 m one we propose here. A dynamic range of 10^{-8} allows detection of objects at contrasts higher than 10^{-8} in the whole field except in the spikes, as the limiting factor is the variance of the noise, not the background residual light, which can be subtracted in the recorded images using a reference source. In one of our recent publications [04] we present simulations of exoplanet detections with contrasts of 10^{-9}. A coronagraphic focal instrumentation will further improve this dynamic range.

II Introduction

The class L mission we propose is a two spacecraft Formation-Flying telescope: the "Fresnel Interferometric Imager" orbiting the L2 Earth-Sun Lagrangian point. It will address different themes of the Cosmic Vision plan, within the guideline questions: “What are the conditions for planet formation and emergence of life?” and “How did the Universe originate and what is it made of?” (see section "scientific objectives").

Proposals for using Fresnel zone plates in formation-flying conditions in space have been made since 1993: Y.M. Chesnokov [05], R.A. Hyde [02], J.T. Early [06], and D. Massonnet [07]. Normally, diffractive optics are usually very chromatic, and allow observations only in a narrow bandpass. The chromaticity issue has been addressed by Hyde [02], Chesnokov [05], Faklis & Morris [08], and solved using an optical principle by Schupmann [01]. Broadband, chromatically corrected observations are now possible with diffractive optics.

Our proposal differs from the previous ones in several aspects. In 2004, we have proposed an interferometric approach, an orthogonal geometry, the use of vacuum instead of an optical active media, and the high dynamic range applications. The Dynamic range is defined here as the ratio of: the average intensity in the image field outside the central lobe of the Point Spread Function (PSF) and its spikes, over the maximum intensity in central lobe of the PSF.

This Fresnel Imager proposal is by no means as elaborate as, for example the TPF-C (a 4x8 meter ellipse aperture coronagraph) or TPF-I (a four 4m apertures interferometer) studied by NASA, or even Darwin (four 3m apertures interferometer). It shares with these an exoplanet detection capability, but is less specialized for this goal. The 3.6x3.6m size of the array has been chosen to fit unfolded as a rocket payload. It could have been chosen rectangular, for the same reasons TPF-C is elliptical, or larger and foldable. However, our rationale at present is to favour simplicity and feasibility, while preserving first order scientific goals. If a mission proves the efficiency of the Fresnel Interferometer concept, then much larger arrays may be envisioned.

II.1 Spectral coverage

The potential spectral domain of the primary array is very broad, being restrained at short wavelengths by the long focal lengths involved (and by the decrease in reflectivity of the secondary field optics mirror coating) and at long wavelengths by the Planck emission of the opaque material of the primary array. This leads to a 100 nanometre – 10 micrometre "global" spectral domain.

The chromaticity of the primary array operating at diffraction order 1 is cancelled by a secondary diffractive element operating at order –1 in a pupil plane. However, the correction concerns only the light that is collected by the field optics. In order to prevent vignetting, the "local" spectral bandpass has to be limited to
$\Delta\lambda / \lambda$ **= 1,41 D / Cgr** for a zero unvignetted field, and less for large fields, **D** being the diameter of the field telescope (e.g. 68 cm) and **Cgr** the side of the square primary array (e.g. 3.6 m).

The Fresnel Interferometric Imager will cover the spectrum with six adjustable bands from Lyman α to close I.R. with angular resolutions from 7 mas at Lyman α, to 57 mas at 1 μm. These bands provide an instantaneous $\Delta\lambda/\lambda = 0.2$ spectral coverage for a given inter-spacecraft distance. From one band to another, the spectral coverage will not be simultaneous : only one spectral band at a time will be observed in this two-spacecraft formation-flying configuration, the inter-spacecraft distance determining the central wavelength of the observed spectral band.

Six dedicated focal instrumentation channels will cover each a spectral band. They will share the primary Fresnel array and the 68 cm main mirror of the field optics. Downstream, all channels will provide imaging capabilities (860x860), two or three of them will have coronagraphic optics and low dispersion spectro-imaging capabilities, the others will have a high dispersion spectro fed from the center pixels of image the field. Hence, for each channel there will be two detectors, one for broadband imaging and one for spectral analysis of a local zone of the field.

The choice of wavelengths for each band depends on the target missions and will be developed in the following sections. – In the UV : spectro-imaging at high spectral resolution for exoplanet transits, stellar & extragalactic objects. – In the visible : stellar and exoplanet measurements at moderate spectral resolution. – In the IR : young stellar objects and planetary systems.

II.2 Angular resolution

The 7 mas angular resolution at 120 nm wavelength is enough for resolving a planet orbiting at 0.07 AU from a 10 pc distant star. The angular resolution would go down to 0.3 arc seconds at 5µm wavelength, but still allow the resolution of a Jupiter at 3 AU. Once the planet is separated from it's star, direct detection of exoplanetary spectral signatures is possible. The spectral resolution and spectrum S/N in that case will be limited, due to the necessary residual starlight subtraction after detection : The expected rejection rates are in the order of 10^{-8}, whereas planet / star contrasts up to 10^{-9} are planned to be observed.

II.3 Field

Contrarily to the nuller approach, almost all the field will be at rejection rates superior to 10^{-8} and only a small solid angle in zodiacal and exozodiacal lights (the area covered by the PSF and its spikes) are contributing to noise at a given point in the field. Two exposures will be necessary to cover the whole field at high dynamic range and allow exoplanet study, as published in A&A [04].

II.3 Dynamic range

The high dynamic range applications that we have tested on the first generation prototype require that the bandpass does not exceed a +/– 15% difference from the central blaze wavelength of the correcting diffractive lens. The optical tests made in with $\Delta\lambda / \lambda = 0.15$ at the 58 Fresnel zones primary array yield $6\ 10^{-6}$ and the numerical simulations for a 350 Fresnel zone array reach 10^{-8}. A consequent improvement of these values is expected with the implementation (in the optical prototype and in the numerical simulations) of a coronagraphic system. The dynamic range decreases for extended objects and dense fields such as galaxies or angularly extended solar system objects, but the angular resolution remains unchanged.

As the present laboratory tests have been made with a fused silica diffractive lens blazed for 600 nm, further validation tests are required for the UV domain. What will change is the blaze angle, towards lower values. The groove spacing has to be homothetic to the Fresnel zone structure of the primary array, thus is not directly wavelength dependant. Quality of the diffractive corrector is of prime importance for dynamic range, as the light not going into its diffraction order –1 may end up polluting the field. Optical are planned in the soft UV range for the months to come.

III Scientific objectives

III.1 Themes addressed

The objectives presented here correspond to different themes of the Cosmic Vision plan: section 1.1 "from gas and dust to stars and planets", section 3.3: "Matter under extreme conditions", and section 4.2: "The Universe taking shape" (High Z galaxies). Other themes, such as in 2.3: "Asteroids and small bodies", could be explored by high angular resolution and high dynamic range imaging from a near-Earth position, but will not be developed in this proposal.

This mission will observe in the UV, visible and close I.R. domains, using six different spectral channels in the secondary spacecraft optics. The central wavelength of four of these channels will be adjusted to obtain a quasi-continuous coverage from Lyman α to 400 nm, and two additional channels will cover part of the visible and close I.R. The central wavelength of each channel will be adjustable to some extent, but high rejection rates and dynamic ranges will only be achieved close to the nominal wavelength of each channel ($\Delta\lambda/\lambda < 0.2$), λ for each band being determined by the blaze angle of the corresponding chromatic corrector lens.

For a primary array transmission efficiency t = 8% ; the proposed scientific program of the Fresnel imager will correspond to that of an equivalent 1.3 m diameter telescope in terms of collected light and 3.6 m in terms of angular resolution. For point sources, the brightness per unit angle in the PSF is that of a 2.1 m diameter aperture : (this will be the case for spectral analysis of angularly unresolved sources).

In addition to being a possible precursor of very large lightweight apertures in space, the strength of Fresnel imager proposed here is also in its dynamic range and capability to operate over a variable spectral range.

This unique possibility could open two very important astrophysical research domains in which members of our group have considerable expertise and significant discovery results : observations in the far UV and the study of exoplanetary atmospheres.

III.2 Observations in the far UV

Contribution by the *Institut d'Astrophysique de Paris* group (Alfred Vidal-Madjar et al).

The UV spectral range is particularly difficult to reach below Lyman α because of limited reflectivity at short wavelengths. However, this domain provides a unique tool to observe gas in numerous astrophysical objects since there are many strong electronic transitions, including of most of the atomic species, ions and molecules. The study of exoplanetary atmospheres can be achieved using high dynamic range techniques (transit or direct imaging)

Both these subjects fall within the ESA Cosmic Vision AO aimed at either the understanding of the Universe as a whole as well as providing significant steps in the search of other habitable planets.

The spectral domain below Lyman α, from 912 to 1216 Å, is particularly known for its instrumental inaccessibility (observed only via COPERNICUS in the 1980's and FUSE between 1999-2007) as well as for its remarkable richness in atomic, ion and molecular lines. Many of these lines are of very important astrophysical species ranging from the more abundant atoms including H, D, C, N, and O, to ions in several states, as in particular CI, CII, CIII (and CIV in the UV near 1555Å), SiI, SiII, SiIII, SiIV, OI and OVI. The UV also contains some of the most important astrophysical molecules as H_2, HD and CO (see Fig. III.1).

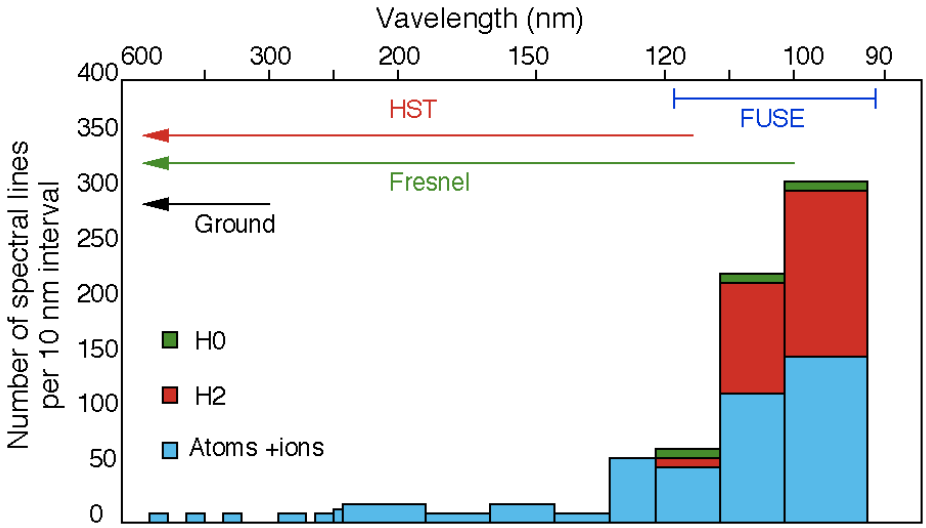

Figure III-1. This figure underlines the spectacular rise in number of available diagnostic lines when moving from the visible to the UV and finally to the far UV (Adapted from FUSE program).

The FUSE observatory was selected by NASA, launched in June 1999, and still operates in orbit (references [10] to [14]). In spite of the technological difficulties, particularly the poor coating efficiencies below 110 nm, the effective area of the FUSE observatory is still "quite high" because only two reflective surfaces were used in its design. The FUSE effective area is on the order of ~50 cm^2, while the proposed Fresnel array, with its 3.6 x 3.6 m^2 collecting area, taking into account the 10% efficiency (wavelength independent) of the diffractive focussing, the efficiency of the two reflection field optics, the additional focal holographic grating as a spectrograph, and a detector efficiency of about 20%, finally achieves a 500 to 800 cm^2 effective area un the far UV. Such a gain, about a factor of 12, should give access to objects 2.7 magnitudes fainter than those presently reached by the FUSE observatory, notwithstanding the gain in angular resolution : 7 milli-arc seconds at Lyman α.

To illustrate a few of the possibilities to be opened by such a gain in sensitivity, one could mention :

– the study of the intergalactic medium observed with FUSE via a small handful of bright quasars and AGNs down to 14th magnitude. The Fresnel interferometric imager would be opened to almost all known similar objects down to 18th magnitude, i.e. thousands of potential targets;

– the study of the galactic elemental abundance in the ISM, presently limited to 13th magnitude hot stars. This study could be extended to 16th magnitude providing access not only to the whole Galaxy, but even to nearby ones such as Andromeda;

– the deuterium abundance, both a unique tracer of galactic evolution and of the primordial Universe, could be evaluated much further in the Galaxy and in more than only one extragalactic target as presently done by FUSE;

– The observation of the physical conditions further inwards from the outer layers of the molecular cloud cores, and their interaction with the ambient radiation field (for instance in dense star forming regions like Orion), particularly in H_2 and CO molecules, will become possible while it is limited for the moment, complementary to the radio observational approach, to the still diffuse envelopes of these molecular clouds; the ionized environment of galaxies, including the cooling flows as traced by the unique OVI lines, could become accessible beyond our own galactic environment to numerous galactic clusters;

– The bright nucleus of the Seyfert galaxy PG 1259+593 has been observed with FUSE. This object of magnitude V=15.84 could be reachable at lower integration times with the Fresnel imager.

– the planetary formation process via the physical state of dense accretion disks, followed by diffuse debris disks, where earth like planets are formed. These processes are particularly well analysed in the far UV spectral range where many important diagnostic lines are available; only a few disks are accessible to FUSE observations.

With a gain in sensitivity of several decades compared to FUSE, a Fresnel telescope would allow scrutinizing the most abundant molecules like H_2 and CO in proto-planetary disks and debris disks much further in the Galaxy and would allow reaching those forming planetary systems in nearby star forming region like in Taurus-Auriga and Orion regions.

Changing the sensitivity of an observatory in a spectral range by a 12 factor is never a trivial step, but in the specific case of the far UV domain, this gain will open up access to most of the possible targets known, changing our vision of any given problem from the current first few hints, to a complete statistical and detailed survey. The targets available in the UV are, even now, all catalogued by the GALEX mission and thus are known to number in the thousands. Moving our observational possibilities in new astrophysical regions always bring new answers and surprises.

III.3 Study of the exoplanetary atmospheres and lithospheres

Contribution by the *Institut d'Astrophysique de Paris* and *Observatoire Midi Pyrénées* groups.

With the study the exoplanetary atmospheres, three possible approaches could be considered:

1 – direct method, trying to observe the light reflected by the planet, and through the spectral analysis deduce the atmospheric and surface composition; this approach requires direct imaging with high angular resolution and rejection rates to properly resolve the planet from the star;

2 – the favourable cases when the planet passes behind its parent star (often called secondary or anti-transit) allowing an evaluation of the amount of planetary reflected light by difference;

3 – the favourable cases when a planet transits in front of its parent star. During these moments, the stellar light passing through the planetary atmosphere gives absorption signatures related to the atmospheric extent, structure, and composition.

These approaches are complementary, one should note interesting advantages of observing transit ***and*** direct imaging or secondary transit:

– direct imaging will add orbital data such as semi-major axes and sin(i), important by many aspects such as obtaining a model independent planet surface temperature. Orbital information may not be available otherwise if there are no transits and if the induced star motion is beyond the sensitivity of Doppler detection;

– when a given planet transits, it also always anti-transits which gives in all those cases the access to the planetary atmosphere, structure and composition over the sunlit planetary atmosphere (secondary transit) as well as its terminators (primary transits);

– the probability of having a transiting planet at about 1AU from a star is ~0.5%. Under the assumptions of a uniform distribution of planetary systems and Earth-like bearing planetary systems in the Solar neighbourhood, if one searches for such planets by direct imaging within 10pc, one should find the same amount of potential targets to be studied via both transit and anti-transit within 60pc from the sun.

Among the lines that could be searched in the transiting exoplanets spectrum, there is :
– Hydrogen at 121.6, Carbon at 130.5 nm, Oxygen at 130.2 and 133.5 nm, 0zone at 300 nm, Na & K at 600 to 900 nm (hot Jupiters), 03 at 800 nm.
– H_2O at 1.8 µm, $C0_2$ at 1.9 µm. NH3 between 3 and 4 µm, CO between 4 and 5 µm.

For direct imaging and spectroscopy, there is need for both angular resolution and high dynamic range in the low part of the light histogram (rejection rate). The spectral windows will be more limited. Furthermore, the reachable spectral resolution for exoplanets with a 3.6 m Fresnel array is as low as 70 with a S/N ratio ranging from 3 to a few hundred (see following figures), allowing detection of the following broad lines :

0_2 at 760 nm, chlorophyl break at 700 nm (possibly at different wavelengths depending on the stellar spectrum). Other lines, such as H_2O at 1.4 & 1.8 µm, and CO_2 lines between 4.2 & 4.5 µm could be a motivation to shift the reddest channel further into the I.R.
More lines may be observed further in the IR, but imaging gets harder due to the loss of angular resolution caused by longer wavelengths.

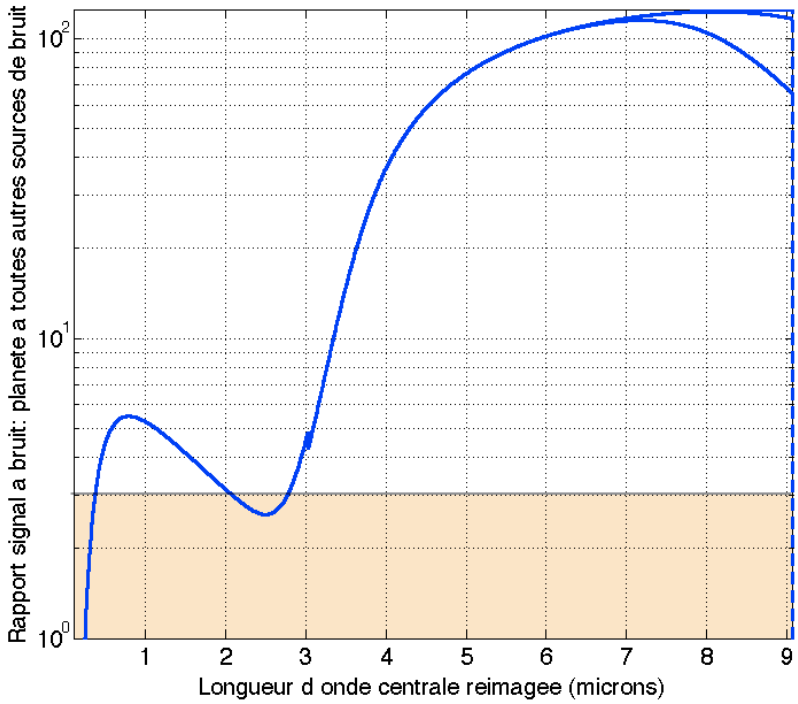

<u>Figure III-2</u>: Signal over Noise ratio as a function of wavelength for a "cold" Jupiter at 5.2 AU from a solar type star, 10 pc away. The shaded zone is where S/N<3. Zodiacal and Exozodiacal contributions are simulated for a solar type planetary system.
24 hour exposure time on a 3.6 m Fresnel array, rejection rate 2 10^{-8}, spectral resolution 70. The star-planet separation allows the angular resolution to be sufficient up to 9 µm. I.R. emission from the planet is observable from 3 to 9µm. The small glitch in the curve at 3 µm is due to a wavelength dependant change in rejection rate, PSF dependant. The thermal emission from the array is taken into account: the bifurcation in the S/N curve at 7 µm corresponds to two different temperatures of the opaque foil: 70K (top) and 80 K (bottom). Numerical simulations by Denis Serre.

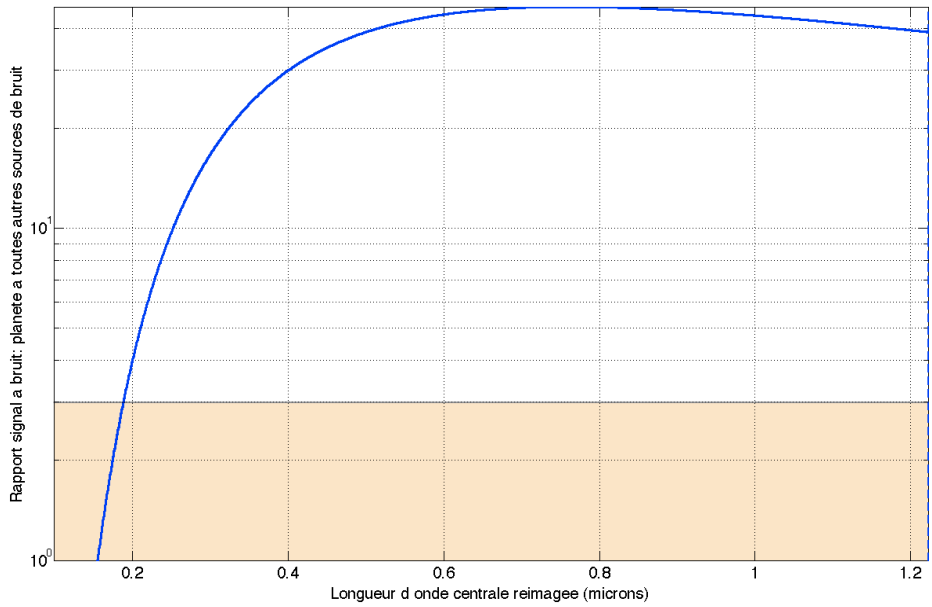

Figure III-3: Signal over Noise ratio as a function of wavelength for a "warm" Jupiter at 1 AU from a solar type star, 10 pc away. The shaded zone is where S/N<3.
One hour exposure time on a 3.6 m Fresnel array, rejection rate 2 10^{-8}, spectral resolution 70. The fall in S/N ratio below 230 nm is due to the decrease in number of photons from the solar type spectrum. At the other end of the observable spectrum, the angular resolution limits the wavelength to 1.6 microns. The shaded zone is for S/N<3.

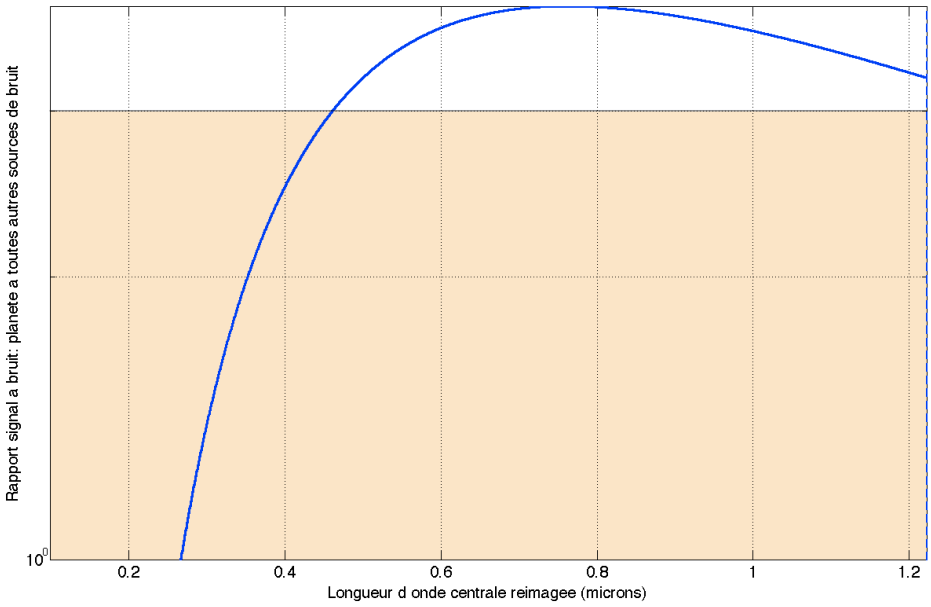

Figure III.4: "marginally reachable" Signal over Noise ratio as a function of wavelength for a Venus at 0.7 AU from a solar type star, 10 pc away. The shaded zone is where S/N<3.
100 hour exposure time on a 3.6 m Fresnel array, rejection rate 2 10^{-8}, spectral resolution 70. The angular resolution limits the wavelength to 1.2 microns. The shaded zone is for S/N<3. An Earth at 10 pc is beyond the reach of a 3.6 m array. It would be marginally reachable, either with a 10 m array at rejection rate 2 10^{-8} , or with the 3.6m array at rejection rate 2 10^{-10}.

In cases 2 and 3 (transit observations: references [15] to [21], and antitransit observations: references [22] to [26]) there is no need for high angular resolution. However, there is need for high dynamic range in the bright part of the spectral lines, and high spectral resolution: the total amplitude of the line variation due to a planet transit like HD209458b is in the order of 10^{-6}, which means a required dynamic range of 10^{-7} if we want to have a S/N of

10 in the planet absorption spectrum.

The important point is that both the transiting and anti-transiting atmospheric planetary studies have already started with both the Hubble and the Spitzer Observatories. In the transit approach, the main Hubble results are the detection of several atmospheric constituents as NaI, HI, OI, CII and H^+ (references) as well as the demonstration of atmospheric escape states as violent as the one probably suffered by the early Earth and Venus, i.e. hydrodynamic escape involving all species transported away within the hydrogen flow. In the secondary transit studies, mainly with Spitzer results, the planetary thermal sunlit side emission has been detected and the temperature and albedo evaluated, as well as the first hints of emission distribution over the stellar-lit hemisphere using timing when the planets disappears behind the star (references are placed after each section). With all these observations completed with instruments (photometers and spectrographs) on board Hubble and Spitzer, it is a simple matter to compare their performances to the present Fresnel Telescope program.

HST - STIS is the best spectrograph used for such planetary studies. The STIS throughput of the different spectrographs ranges from 1 to few percent from the UV to visible and thus corresponds, in the case of a 2.4m diameter telescope, to an effective area of the order of ~500 to few 1000 cm^2. In the case of the 3.6 x 3.6 m^2 Fresnel Telescope, one could again reach, with two-reflection field optics design and a relatively simple one reflection grating design, and a 20% efficiency detector, nearly a 2000 to 3000 cm^2 effective area system, depending upon the spectral range considered. Here a gain by a factor of 3 relative to present observations will allow the same studies accomplished now over 8^{th} magnitude stars to be done in the case of more than 9^{th} magnitude similar objects. It is clear that this will not be enough to reach for potential Earths but will increase the number of atmosphere studied by nearly a factor of 6, i.e. statistical studies could really begin.

This study being made with a 3.6 m Fresnel Telescope, one can hope that if the first mission is successful, further development steps of that design will allow to really reach Earth type planetary atmosphere, using 15 to 30 m Fresnel arrays. See as a prediction of the possibilities the following Table III-1, taken from the Lecavelier des Etangs and Ehrenreich (2005) Cosmic Vision proposal.

Planet Type	Telescope ⌀ (m) for V=8, S/N=5			Number of targets (S/N≥5, ⌀=10m)
	K-star	G-star	F-star	(N/$\beta\gamma$)
Earth	15	22	29	14
Venus	50	83	113	<1 (0.3)
Ocean-Planet	2.3	4.4	6.8	3400
small Earth	9	13	17	61
small Venus	36	64	92	< 1 (0.9)
small Ocean-Planet	1.4	2.7	4.0	13 900
super-Earth	65	113	142	< 1 (0.1)
super-Ocean-Planet	9	18	29	54
Hot Jupiter	2.0	3.5	5.5	40 000
Hot Neptune	9.0	17	25	440
Evaporating ocean	<1	<1		1 150 with ⌀=1m
Evaporating ocean				590 in Local Bubble

Table III-1: Taken from Lecavelier des Etangs and Ehrenreich (2005) shows the number of planetary targets accessible with an equivalent to 10m diameter telescope. Although this looks like a remote possibility in the case of a classical 10 m space telescope, a 30 m Fresnel array having the same colleting power and triple angular resolution may be a relatively simpler solution.
Using the approach of Ehrenreich et al. (2006) we have adapted the evaluation of the detectable planets to a 30m Fresnel array as a follow up of our program. We included all varieties of known extra-solar planets from Earth sized planets to Jupiter-like planets, adding their probable satellites, as well as possible Ocean planets and Early Venus or Evaporating ocean type planets. This table demonstrates the huge potential capabilities of our design which will still show important (in statistical terms) detections with the present proposed size of 3.6m in the easiest cases since at the time of this program operations, many more transiting planets will be known thanks to the large number of present and/or future ground based (e.g. OGLE, TrES, XO, HAT, etc...) and/or space borne programs (e.g. CoRot and Kepler ,etc.) aimed to transiting planets.

III.4 Study of stellar systems, photospheres and close environments

Contribution of Margatita Karovska, *Harvard Smithsonian Center for Astrophysics*. *references [27] to [28]*.

Since 1990s the Hubble Space Telescope (HST) has been providing high-angular resolution views of the Universe from UV to IR wavelengths with an angular resolution close to 0.1 arc second. The diffraction limit of this 2.5m telescope is comparable to the ground-based telescopes built over 50 years ago (e.g. Mt. Wilson 2.54m telescope). However, the fact that the HST is in space and therefore free of the atmospheric seeing effects, with the crucial capability of observing at UV wavelengths, provided unprecedented opportunities for high-resolution studies of many astronomical sources. For example, HST observations of the nearby symbiotic system Mira AB (at 130pc) demonstrate the power of sub-arcsecond angular resolution by having separated the components of this 0.6" interacting binary for the first time at UV wavelengths where the most important signatures of accretion occur (Karovska et al. 1997) Mira AB is the nearest symbiotic system composed of an evolved mass-loosing AGB star (Mira A) and a wind-accreting white dwarf. HST and Chandra images of Mira AB showed evidence for possible direct interaction between Mira A and its companion, showing that Mira B is accreting not only from the wind of the AGB star, but also via direct mass exchange (Karovska et al. 2006). This was an unexpected result, because the components are separated by 70 AU and it has been assumed in the past that the interaction between the components in such a system can be carried out *only* via wind accretion.

Unfortunately, very few interacting binaries have been resolved by direct imaging from the ground or from space. Currently, most of our accretion paradigms are based on time-resolved spectroscopic observations. An order of magnitude higher (10 mas) spatial resolution in the UV and optical will offer unprecedented opportunities for detailed studies of nearby stars and interacting binary systems.

The Fresnel Interferometric Imager (FII) will be able to image the Mira AB system with 100 pixels covering the region between the components, and 100 pixels covering the atmosphere of Mira A. Furthermore, the FII will be able to separate the components of several nearby currently unresolved interacting binaries, including symbiotic systems (e.g. CH Cyg, R Aqr, and others). Symbiotics are some of the most fascinating interacting systems because of their dramatic transformations and extremely complex circumbinary environment. These systems are very important because they are likely progenitors of bipolar planetary nebulae. They have also been invoked as potential progenitors of at least a fraction of Supernovae type Ia, a key cosmological distance indicator (Chugai 2004).

Furthermore the FII will be able to resolve outflows and the circumbinary environments in a variety of systems, including regions of colliding winds. The results will have important implications for our understanding of accretion processes in detached binaries and in other accreting systems in the Universe. Understanding accretion driven flows in binaries will directly affect our understanding of similar flows around YSOs, including the formation of planets in the circumstellar disk.

The HST and ground-based observations detected significant asymmetries in the atmospheres of several nearby giants and supergiants, including in Mira A and Alpha Ori. However, the causes of these asymmetries remain a mystery. Possibilities range from giant stellar spots, convective cells, to effects of non-spherical pulsation and massive outflows. Resolution of an order of a magnitude higher than that of the HST in the UV is needed to determine the causes of asymmetries observed in these evolved stars. The FII will be able to image the atmospheres and the circumstellar environment of dozens of nearby Mira-type stars and supergiants with approximately 100 pixels over the stellar surface, compared to only few that we currently get using the HST. This will allow determining the causes of the asymmetries and also a detailed study of the structure of the extended atmospheres.

III.5 Study extra-solar protoplanetary disks: The Disk Evolution Watcher (DEW)

Contribution of Prof. Ana I. Gomez de Castro *Universidad Complutense de Madrid*

Observations of extra-solar protoplanetary disks allow understanding the physical evolution and chemical composition of disks at epochs preceding and contemporaneous with the formation of planets. Chemical abundances are determined by physical conditions such as density, temperature and the incident radiation field. The UV radiation field plays a fundamental role in the chemical evolution of the disks:

-1. FUV continuum emission induces photodissociation of CO enhancing organic species such as CN, HCN and HCO+ (Aikawa and Herbst, 1999, 2001).

-2. Lyman alpha carries about 85% of the far UV energy flux (see TW Hya observations by Herczeg et al 2004 [32]). Thus the radiation field is selectively dissociating species like HCN or H_2O while others such as CO or H_2 are left unaffected (van Dishoeck et al 2006).

-3. The vertical structure of the disk is controlled by the UV radiation of the central source. The disk can be divided into three layers: the upper Photo-Dissociation Region (PDR), the warm molecular layer below and the mid-plane cool layer. Low molecular abundances are caused by depletion in the mid-plane.

-4. The structure of the inner disk (r<2 AU) is controlled by the evolution of the accretion-outflow engine. The engine transforms gravitational energy into mechanical energy (the outflow) and radiation. The presence of magnetic fields makes the dissipative processes to occur at high energies (UV, X-ray radiation) compared with the temperature of the disk and the stellar photosphere. This radiation, in turn, controls disk evolution (see [31], for a recent review).

The Fresnel Interferometric Imager (FII) has the following properties that make it an ideal instrument to follow the evolution from disks to planets:

-1. The high dynamical range allows to map simultaneously the illuminating radiation field and its propagation / diffusion in the circumstellar environment. A 1e7 dynamical range makes feasible to track the radiation field to a distance 3.2e3 times the radius of the illuminating source. Assuming this to be the central engine (with a characteristics radius of 10 stellar radii or 0.05 AU), the FII will allow to map with unprecedented sensitivity and resolution the inner 100 AU with a resolution of 7mas (0.98 AU at 140 pc, the distance to the Taurus or Lupus, the nearest nests of Pre-Main Sequence stars). This scale reduces to 0.098 AU for AB Dor (a nearby Weak-Line T Tauri star) or to 0.392 AU to TW Hya. For this objective, possible problems caused by zodiacal light will have to be investigated (Taurus is in the ecliptic).

-2. The high dynamical range and resolution allows to map the inner region jet with unprecedented resolution and measure the role that the jet may have in the illumination of the inner region of the disk. The simulataneous observation of the jet and the engine will allow to track the correlation between engine and jet variability and derive parameters such as the knots excitation and jet collimation mechanisms.

-3. The possibility to obtain simultaneously the spectra of the central source and the high resolution image allows to measure the relative contribution of the various lines to the illuminating flux: Lyman alpha, OI, CII and CIV for the Far UV and provide direct input data on the selective absorption role on the chemical evolution of the disk.

-4. The possibility to observe in several spectral windows, extending towards the IR, will allow to map the effect of the irradiation field on the disk atmospheric structure (the warm molecular layer) where CO, CO_2, H_20, NH_3 emission is observed. Also the role of the UV radiation field in PAH formation could be studied since some of the most prominent PAHs molecular bands are within the range of the FII. FII will also sprovide direct information on the extinction law (from 100nm to 10000 nm) and the properties of the dust lifted from the disk at different locations providing crucial information for future projects like ALMA.

III.6 Extra-galactic program with the Fresnel Interferometric Imager

Contribution of Roser Pello *Observatoire Midi Pyrénées*

Several extragalactic projects could be addressed with the proposed Fresnel Interferometric Imager (hereafter FII). These projects take advantage of the outstanding capabilities of FII in terms of spatial resolution, wide wavelength domain and high dynamical range as compared to other ground-based and space facilities available or planned beyond 2012-2015. FII is intended to start operations after JWST, ALMA and possibly SKA. Therefore, extragalactic science with FII has to be optimized to take maximum benefit from synergy and complementarity with these ongoing projects. FII is expected to substantially contribute to a new panchromatic view of galaxies at all redshifts, thus providing new clues to understand galaxy formation and evolution.

This is a non-exhaustive list of extragalactic projects which could be addressed with FIIs:

– Evolution of the Star Formation activity in the Universe: a complete census from high-z to the local universe:

Thanks to its UV to near-IR imaging capabilities with optimal spatial resolution, FII is an ideal instrument to study the evolution of star formation activity, traced by the restframe UV flux, from the early epochs to the

present-day universe. Indeed, JWST is an infrared-optimized space telescope, hence the UV capabilities of FII are particularly well suited to determine the energy census of galaxies at all redshifts, in particular from the mid-z (z<~2-3) to the local universe. The expected impact of FII in this area could be easily evaluated by extrapolating the recent results of GALEX, the only facility presently available (and foreseen) in the UV. FII is expected to complement and to extend the capabilities of GALEX. Because of its small FOV and high spatial resolution (typically one galaxy per shot), FII is intended to be a follow up rather than a survey instrument. FII could be efficiently used to target galaxies selected from utra-deep photometric and spectroscopic surveys (optical + near IR).

– Mapping the Star Formation of galaxies in the local Universe.

The high spatial resolution of FII in the UV to near-IR could be used to obtain a detailed mapping of the star-formation activity in the local Universe, both in imaging and spectroscopic modes. An unprecedented resolution could be achieved in the study of the physical properties of star-forming regions by combining the spectroscopic information provided by the ISM and stars in these regions.

- Exploring the AGN-starburst connexion.

The relationship between AGN and starburst activity in galaxies is a very important topic, closely related to the process of galaxy assembly across the cosmic time. Starburst (or post-starburst) activity is usually located around the central AGN. FII could provide a new insight into this subject thanks to its high spatial resolution at all wavelengths from UV to near-IR, and to its very high dynamic range.

- Observing the first galaxies with FII : Constraining the physical properties of galaxies at z>7

This project is focused on the spectroscopic study of a sample of ``bright" z~7-12 galaxies, for which we could take advantage of the spatial resolution provided by FII in the near-IR. This is also a test case for an improved version of FII with a larger aperture, which could sustantially improve the capabilities of JWST for the study of the first galaxies in the Universe. Indeed, most z~7-12 galaxies are expected to have an angular size below 0.1". The physical properties of such distant galaxies could be derived from Lyman alpha emission, combined with multi-wavelength photometry. Two different cases could be explored in this prospective phase :

High-z galaxies selected around the critical lines in mid-z strong-lensing clusters. In this case, the FOV of FII in the near-IR is ideally suited for this study. The detection of magnitude-limited samples of z>7 galaxies is a factor between a few and a few*10 times more efficient in lensing clusters than in blank fields (depending on FOV - especially for a FOV of ~1-2'!-, redshift of lenses and sources, LF of sources ...), and the relative efficiency increases with the redshift of the sources. The survey could be either "blind" (because the position of the critical lines at such high-z are known with well suited accuracy), or "pointed" after the photometric pre-selection of candidates found in previous (ultra)deep surveys of lensing clusters. The later is better suited for the prospective phase.

High-z galaxies selected in blank fields from previous studies. Utra-deep optical+near-IR surveys (broad-band filters) are presently ongoing or planned, using different wide-field IR cameras. The new generation of ground-based near-IR spectrographs should be able to confirm the most promising "bright" candidates. However, the combined gain of FII in spatial resolution and ideal spectral resolution could be crucial to confirm a fraction of the fainter candidates, as well as a privileged test-case for the next version of this telescope.

III.7 Conclusion

The scientific program with a Fresnel Imager presented above covers the "short wavelength" part of its observable domain. This choice has been made because of the intrinsic richness of physical phenomena in the U.V., and also to take advantage of the larger angular resolutions induced by short wavelengths, allowing competitive resolutions with a modest 3.6m aperture. If in the future larger Fresnel arrays are envisioned, there will be many targets in the spectrum up to 10 μm, and sufficient angular resolution to realize for example exoplanet study in the IR.

The Fresnel imager can be considered as an "aperture multiplier": it uses a modest dimension two-reflection solid aperture telescope as field optics, onto which light is focussed form upstream, by a diffractive aperture array five to ten times larger in diameter. This Fresnel array provides the angular resolution, imaging capabilities and wavelength independent focussing efficiency (independent in terms of transmission, not focal length) of a

large aperture, without the manufacturing and weight constraints of building and launching a large mirror. Future space telescopes of this type using 50 to 100 meter foils could lead to sub milli arc-seconds resolutions with two-vessel formation flying systems having 4 to 400 kilometre focal lengths. These future missions could be an alternative to large solid aperture space telescopes or multi-telescope space interferometers.

In case of large arrays, formation flying with more than two spacecrafts would allow simultaneous observations at two or more spectral bandpasses, each spacecraft being at its corresponding focal length along the optical axis. Central obscuration would occur with the present centred Fresnel design for the last-in-row receptors. Off-axis Fresnel arrays solve this shadowing problem, at the cost of an increased manufacturing precision and number of subapertures.

Due to the long focal lengths of Fresnel arrays, their aberration-free field of view is large: a fraction of a degree. It could even be envisioned to increase this field of view to a few degrees with the use of aberration correctors in the focal optics. There is no point to increasing the field of view if it cannot be covered by focal optics. However, this would allow sharing a unique primary array for a simultaneous multi target mission in the same region of the sky, undertaken by several secondary spacecrafts. This very prospective paragraph and the two above are not to be taken too seriously for now, it's just here to show that "we too" can propose futuristic multiple spacecraft missions.

IV Mission profile proposed to achieve these objectives

Several points presented in this section are developed in more detail at section V.

IV.1 Primary optics

The primary optics will consist of a square Fresnel interferometric array, 3.6 x 3.6 meters. This is the maximum size allowed without folding into the payload compartment of a large launcher. Folding would allow larger apertures, but would require deployment systems to be developed, and add technological hazards to the already challenging formation flying and light foil aspects of this mission.

The "Fresnel number" (number of Fresnel zones) of the proposed 3.6 x 3.6 m array, in the following noted **N**, is 600 to 800, leading to a minimum of 2.88 million subapertures interferometer. The total cutting length, L, required to carve all the subapertures is 8.6 km for a 3.6 m array. This length grows proportionally to the Fresnel number (i.e. as the square root of the number of subapertures) : $L = 4NC_{gr}$, where C_{gr} is the side of the square Fresnel array.

The estimated cutting time, assuming the same laser technology as the one used for the prototype, is 466 hours. The largest (central) pattern is 100 mm in size, the smallest (limb) patterns are 0.5 to 0.7mm.

The weight would be in the order of 200 kg for a 0.8 mm thick stainless steel foil, 3.6 x 3.6 m^2, not taking into account the frame and baffle. This is just an example extrapolated from our lab prototype, the phase zero work started at CNES on the project should evaluate other materials.

For an extended source, the diameter D of a 100% efficient circular aperture yielding the same luminosity as an array of size C is given by: $D = 4/\pi\ C\ t^{1/2}$, where t is the transmission efficiency of the array at order 1; For a 3.6 square array, this corresponds to a 1.3m diameter mirror. (assuming a t=0.08 transmission into order 1).

For an unresolved source, the average illumination per unit angle in the PSF of a Fresnel array corresponds to that of a 100% efficient circular aperture of diameter $D = 1.1\ C\ t^{1/4}$, this corresponds to a 2.1 m diameter mirror, at t=0.08.

The diameter of a circular aperture telescope yielding the same angular resolution is between 3.1 and 4.4 m, depending of the orientation in the field, the PSF support being square. The best direction angular resolution is respectively 5.7 to 57 mas at λ=100 nm to 1 μm.

IV.2 Secondary optics

The secondary optics consists of a "field telescope" 68 cm in diameter. This telescope plays the role of a field lens. It could be a 2-mirror Cassegrain off axis combination. It is placed near the focal plane of the primary array. Its does not image the sky, but re-images the primary array onto a pupil plane, where the chromatic corrector is placed.

The field mirror diameter is driven both by the desired spectral bandwidth per channel and by the desired field. With a 68 cm diameter "field mirror" one can achieve a 900 x 900 field / resolution ratio at the central wavelength of each channel or an unvignetted 27% relative spectral bandwidth at the centre of the field, or any combination thereof. Going beyond these limits starts causing vignetting.

All channels will share the first reflecting mirror of the field telescope. Depending on the attitude of the secondary spacecraft, the beam will be sent on different secondary field mirrors and the pupil will be imaged over different optical channel correctors and detectors, each optimized for a given spectral band.

There will be six wavelength channels from 100 nanometres to 1 microns, each with a 27% relative spectral bandwidth. A 10^{-6} to 10^{-8} dynamic range allowing detection at higher contrasts and a detector adapted for sampling the 800*800 resolution elements field spanning from 5.7 to 57 mas, depending on the wavelength.

IV.3 Formation flying requirements

The mission lifetime expected is ~10 years, extendable to 15 years. Long lived formation-flying missions with kilometric distances require low gravity gradients: obtained either at L2 or L1 Lagrangian orbits.

IV.4 Launch

Due to the frame size of the primary optics, the launcher recommended is a large payload and medium mass (2000 kg) capability one, such as **Soyuz**. The weight should not be a critical parameter, particularly for the Fresnel Interferometric foil.

1. Launch from **Kourou**.
2. The spacecrafts are injected in transfer orbits to L2.
3. Soyuz and both payload spacecrafts all separate from each other.
4. Spacecrafts fly separately to L2. The travel could last from 3 to 6 months.
5. The first formation-flying tests can be achieved during the transfer phase.
6. Both spacecrafts undergo continuous orbit corrections to reach the final orbit.
7. Injection to final orbit around L2.

IV.5 Orbit requirements

The L2 orbit proposed is a halo or Lissajous type orbit. The spacecraft holding the Fresnel array and baffle will be applied periodical orbit maintenance corrections, the secondary spacecraft holding the field optics, spectral channels and detectors will be set to follow the primary at the position required by the focal length and optical axis direction.

IV.6 Ground segment

The ground segments needed would be the same as for other Lagrangian point operations.
As for the Ground Station, this mission would use the 15 m antennas (Ex : Kourou, transmit bands : S&X).
It is to be defined in cooperation with the different members of our group.

V Proposed payload instrument complement required to achieve science objectives

The proposed two-spacecraft formation-flying Fresnel Interferometric Inager is as follows:

A first spacecraft constitutes the "**Fresnel Array Spacecraft**".

This spacecraft holds the primary optics of the telescope: the Fresnel interferometric array. It gathers incident light and focuses it into an intermediate image plane where the second spacecraft is located. Because it stands for the entrance pupil of the instrument, its dimensions drive the angular resolution and its geometry determines the dynamic range.

A second spacecraft constitutes the "**receiver spacecraft**".

This second spacecraft holds the secondary optics of the telescope. It receives the light coming from the primary optics and images the target onto detectors, adapted to six different spectral bandwidths. Likewise, it removes some geometrical aberrations due to the primary diffractive optics, such as chromatism. Its dimensions determine the angular field and spectral coverage within each channel.

V.I Overview of the proposed payload elements:

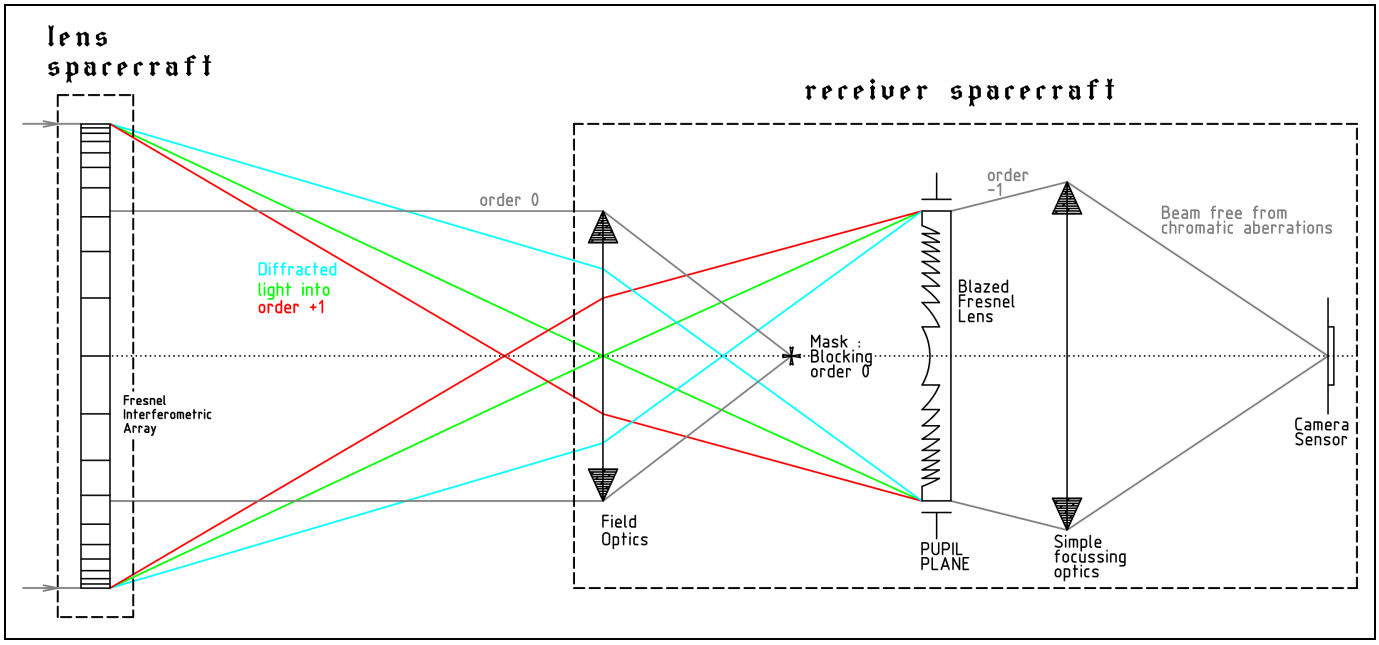

Fig V-1: principal payload elements and ray propagation inside the instrument. The two modules are not at scale in this figure.

The principal payload elements and the ray propagation are depicted in the figure above (Fig V.1) :

A parallel beam coming from the astrophysical object hits the first payload element: the Fresnel interferometric array protected on its sides by baffles. It behaves like a grating that focuses light by diffraction using a large number of void subapertures punched in a thin opaque foil. Because this is binary optics, we get positive diffraction orders (+1 ; +3 ; +5 ...) which produce real images, negative ones (–1 ; –3 ; –5...) which form virtual images, and finally order 0, which yields a parallel beam.

This Fresnel interferometric imager takes advantage of the **order +1**: it is the most powerful of the diffraction orders, higher diffraction orders have negligible energy; and it makes a real image. Notwithstanding, this order +1 image is not directly workable, owing to its strong axial chromaticity. Indeed, the product of the wavelength by the focal distance is a constant: the focal plane gets further as the wavelength is shorter. Such an aberration would cause a blurred PSF except in very narrow spectral bandwidths.

We achieve broadband imaging with a complete correction of the chromatism, by means of a second diffractive element placed in a pupil plane, which, operating at diffraction order –1, applies a rigorously opposite chromatic aberration to that of the Fresnel array. The wavelength dependence of the final focal plane is thus cancelled. Initially L. Schupmann in [01] and later R. A. Hyde in [02] proposed this chromatism correction principle.

We have implemented and tested an evolved version of this optical corrector in our prototype.

Two principal payload elements are needed to achieve the chromatic correction: field optics and a blazed Fresnel lens.

– The field optics has two major roles in the correction scheme : first, gathering the whole focused beam from the order +1 of the Fresnel interferometric array, for a given spectral bandwidth ($\Delta\lambda/\lambda \approx 0.3$). Second, to reimage the primary Fresnel array onto a "pupil plane" where the next element of the optical train is located: a special diffractive Fresnel Lens.

– A mask is placed at the focus of the field optics in order to block out the fraction of the parallel beam order 0 from the primary Fresnel array that ends up onto the field optics. This is required for high dynamic range imaging.

– The small blazed Fresnel Lens is a diffractive optics that operates at **order -1** and compensates for the chromatic aberrations. Its Fresnel zones and those of the primary Fresnel array are homothetic. We obtain at this level a divergent but corrected beam, free from chomatism.

– A convergent relay optics, which shed the image on the detector.

– Finally, we get a camera sensor in the focal plane, at which coronagraphic or spectrographic add-ons can be appended.

V.2 Detailed Payload elements and their function :

The "Fresnel Array Spacecraft", holds: the Fresnel interferometric array and its baffles and solar panels, guidance equipment for alignment and attitude control, inter-spacecraft communication equipment.

V.2.1 Baffled Fresnel interferometric array: it is the key element.

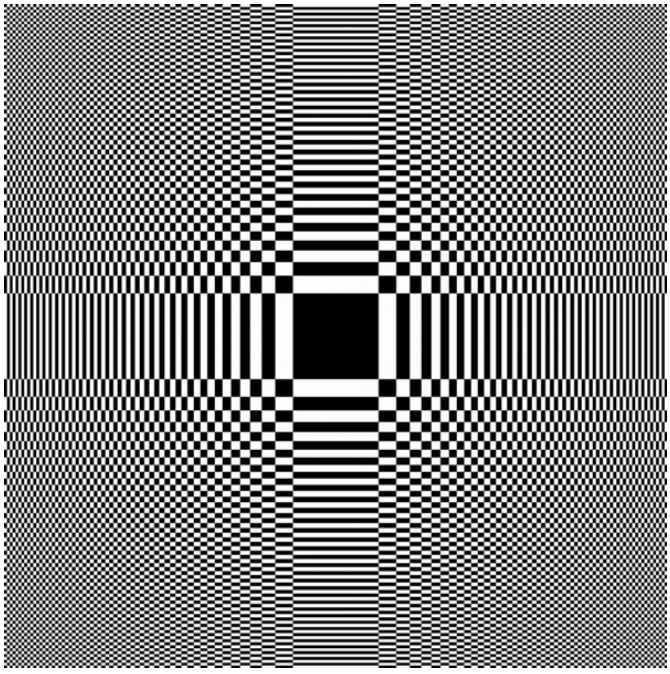

Fig V-2: Our orthogonal Fresnel array geometry.

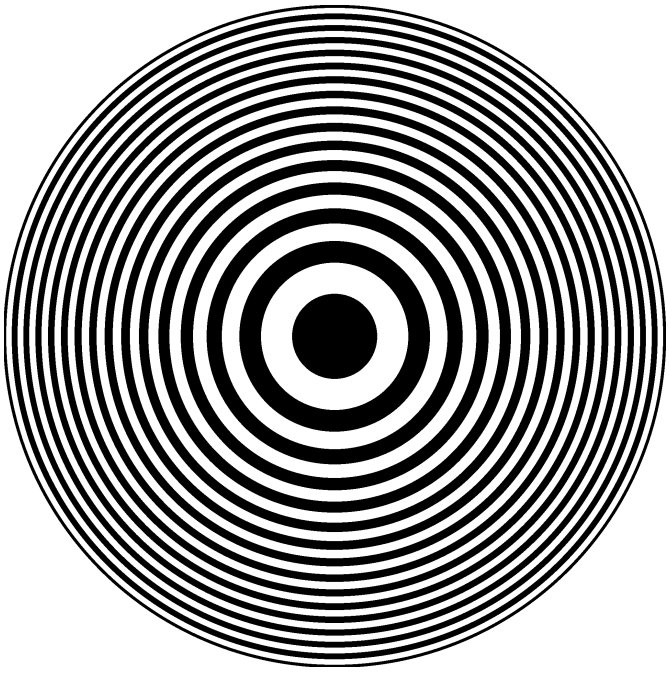

Fig V-3: Standard circular amplitude Fresnel zone plate.

The Fresnel interferometric array we have designed is the orthogonal pattern shown in Fig V.2. It is not a classical amplitude Fresnel zone plate as illustrated in Fig. V-3. However, other subaperture patterns, beyond orthogonality, are studied, which should improve both transmission and dynamic range.

This thin and lightweight focussing foil can be seen also as a dense interferometric array. Its design has been explained in depth in [04]. Two key parameters characterise these optics:

– N : The number of Fresnel zones along orthogonal axes Ox and Oy.

A Fresnel zone is a concentric rim within which the range of optical phase variations, as seen from order +1 focus, remains bounded in $[-\pi ; \pi]$ interval. Therefore, the optical path difference between outline circles of

neighbouring Fresnel zones is one wavelength (if computed from order +1 focus). In each Fresnel zone of this focussing array, there are neither reflective nor refractive elements, but a set of opaque or void patterns. The latter are specifically carved and positioned to block out the non-desired wavefront phases so as to combine constructively the beam in a common focus and yield a real image. Of course, the connectivity of opaque patterns is required to achieve mechanical self stability of the array. Numerical simulations show that the Fresnel number N is particularly determinant for dynamic range. The larger N is, the higher the resulting dynamic range in images. An N = **600 to 800** array seems to be reasonable for that mission and could reach $\mathbf{10^{-8}}$ dynamic ranges, allowing detections of objects at 10^{-10} contrast in favourable cases.

– Cgr : The side size of the square array.

This parameter determines the angular resolution, ρ_{min}, of the imager:

$$\rho_{min} = \lambda / Cgr$$

where λ is the considered wavelength. The larger the Fresnel array, the better the resolution limit. Yet, for this mission, we propose an array size of 3.6 m to simplify deployment issues. Future space telescopes of this type could use **50** to **100** meters Fresnel arrays, leading to the micro arc-second resolution domain presently reserved to diluted array interferometers in the radio domain (e.g. VLBA).

The parameters presented above establish the focal length $f(\lambda)$ of the Fresnel array at order +1 :

$$f(\lambda) = Cgr^2 / (8\ N\ \lambda)$$

The $f(\lambda)$ expression specifies the flying distance of the "receiver spacecraft", which depends on the central wavelength (λ_C) of the desired spectral bandwidth. In the proposed configuration, this flying distance has a maximum span of from **2.5 km** in I.R (1µm) to **18.3** kilometres in U.V (127 nm).

Two other parameters play an important role in the Fresnel interferometric array :

– The global amplitude apodization functions of the Fresnel array. These are weighting functions applied to the subaperture sizes that diminish them with respect to their nominal value from center to limb of the array. The purpose is to enhance the dynamic range near the center of the Point Spread Function (PSF). See [04]. We have implemented and tested this apodization scheme in our prototype. Only mild apodizations can be applied that way, due to their effect on lowering array transmission. Other apodization techniques, which are not altering transmission, will be investigated, such as Guyon or PIAA (Phase Induced Amplitude Apodization). These apodizations will be applied in a pupil plane within the secondary optical trains.

– The individual subaperture shapes : A pseudo-fractal cutting achieving local apodization of each subaperture could increase the order +1 focus transmission efficiency. Other patterns are investigated to realize a sine apodization : the order +1 light efficiency would thus reach 12%.

At present, we use a two-dimensional orthogonal array geometry (Fig V.2) with mere rectangles as subapertures. For an array designed at wavelength λ_0 and focal distance f_0 in order +1, the transmission law Tc(x,y) is defined as follows :

$$T_c(x,y) = h(x)g(y) + g(x)h(y) \quad with\ \ h\ \ and\ \ g\ \ defined\ as:$$

$$g(u) = 1 \quad if \quad \sqrt{u^2 + {f_0}^2} \ \in \ \left[(k + \frac{f_0}{\lambda_0} + \frac{1}{2})\lambda_o \, ; (k + \frac{f_0}{\lambda_0} + 1)\lambda_o \right] \quad and\ g(u) = 0\ \ otherwise$$

$$h = 1 - g$$

In this configuration, the maximum efficiency at order +1 is $E_{max} = 4/\pi^4$, that is 4.1 % for a non-apodized array. This is what we get with our present optical setup using raw orthogonal geometry. We are currently working on higher transmission geometries that should increase the order +1 transmission to 10%, They should be tested before the end of 2007. For the numerical simulations in the "scientific objectives" part of this proposal, we have set the transmission rate to 8%.

V.2.2 Tolerances in positioning and surfacing of the main array:

For this kind of grating, with a *f* focal distance, the Optical Path Difference error (ΔOPD) is approximately given by $\Delta OPD = \frac{x\Delta x + y\Delta y}{2f} + \Delta z \frac{x^2 + y^2}{4f^2}$ where (x , y) are the coordinates in the array plane, (Δx , Δy) the subaperture mispositioning, and Δz the subaperture mispositioning in the perpendicular (propagation) direction. The maximum error entailed appears for defects in the corner of the array, that is for x = C/2 and y= C/2. This leads to an ΔOPD upper bound for the perpendicular plane. We get $\Delta OPD(\Delta z) < \Delta z \frac{8 N^2 \lambda^2}{C_{gr}^2}$ at Δx and Δy nil. The second upper bound is at Δz nil for the array plane : $\Delta OPD(\Delta r) < \Delta r \frac{2\sqrt{2}\, N \lambda}{C_{gr}}$, $\Delta r = \sqrt{\Delta x^2 + \Delta y^2}$. The ΔOPD(Δr) constraint is the most severe of the two.

We have accomplished a comparison among the tolerances of three kinds of optics in Table V-I: mirror, lens and Fresnel interferometric array. It emerges that the surface accuracy constraints are dramatically relaxed for the latter.

	Thin silica lens n=1,5 with surface error Δz	***Mirror with surface error Δz***	***Fresnel array with subaperture position error (Δx , Δy , Δz)***
Wavefront error formula (ΔOPD)	Δz (*n* – 1)	2 Δz	$\frac{x\Delta x + y\Delta y}{2f} + \Delta z \frac{x^2 + y^2}{4f^2}$
For N = 700, Cgr = 3.6 m λ = 600 nm	0.5 Δz	2 Δz	$3.3\ 10^{-4}$ Δr *and* $1.09\ 10^{-7}$ Δz
To generate a λ/Q quality wavefront, we need :	Δz < 2λ/Q	Δz < λ/(2Q)	$\Delta r < \frac{C_{gr}}{2\sqrt{2}\, N Q}$ (independent of λ)
Tolerance for Q=50	**λ/25**	**λ /100**	**> 120λ** *(for λ=300 nm)*
Pick-valley tolerance for *(for λ=300 nm)*	12 nm *(for λ=300 nm)*	3 nm *(for λ=300 nm)*	**36 µm**

Table V-1: Compared tolerances involved to realize a given pick-valley wavefront quality for three types of optics. Q is a measure of the tolerance on the optical surface, expressed in inverse fraction of the wavelength. For reflective or refractive optics, the tolerance for a given wavefront quality is proportional to the wavelength, whereas for a Fresnel array, this tolerance is not wavelength dependant.

The PSF of such a Fresnel array is computed in Fig I.2 and Fig I.4. It seems suitable for high-contrast compact-object imaging such as exoplanets. Owing to its orthogonal-only subaperture edges, light escaping the central lobe of the PSF is mostly confined within two orthogonal spikes, whereas that of standard circular Fresnel zone plate, or to a lesser extent solid aperture, undergoes an isotropic dispersion in concentric rings. Hence, for a Fresnel array, the spatial energy distribution yields four field quadrants at very low stray light level and therefore enables a high dynamic range imaging in all the field except the spikes.

We simulated that the PSF remains insignificantly aberrated until a 0.3 degree of field.

To conclude with this main payload element, we summarize its most important assets and drawbacks in Table V-2.

property	***Assets***	***Drawbacks***
Focussing light by diffraction using an all-or-nothing transmission (binary optics).	Apodization can be easily performed in entrance pupil.	Low energy efficiency at focus, less than 10%.
	Exactly the same angular resolution as that of monolithic aperture of identical size.	
	Mere vacuum as subapertures: this eliminates mostly of phase defects. Focussing light by diffraction allows a broad working spectral domain spanning from U.V to I.R.	Very weak optical power, which involves long focal lengths. They become huge as the wavelength approaches far U.V and lower wavelength domains.
	Concerning the accuracy of subapertures carving, fabrication constraints should be strongly released. In situ, the wavefront quality would be relatively insensitive to array warping or distortion.	Strong chromatism that should be corrected.
Orthogonal geometry of the array structure.	Mechanic cohesion of the whole optics.	Low energy efficiency at focus: 4%. Can be improved to 8 or 10% by enhanced pattern design
	Parasite energy confined into two orthogonal spikes of the PSF : improves dynamic range for compact objects.	
Large number of subapertures	Enhances the dynamic range and enlarges the "clean field".	Because the Fresnel array foil is very thin and large and has a hollow structure, it might be very fragile. This could complexify launch and deployment issues, as well as the array fabrication.
	Higher field / resolution ratio. Allows much wider fields than other interferometers [03].	

Table V-2: Summary of main assets and drawbacks of the Fresnel interferometric array

Two lateral baffles will prevent Sun or Earth light from hitting the Fresnel interferometric array. They will be large enough to enable a plus our minus 20 degrees angle between the Sun direction and the array plane. For a 3.6 m sized array, this is a 1.3 m tall "wall" at two at least of the four sides of the array, above and below. These baffles should be slightly tilted outwards, to prevent diffused light to reach the secondary optics.

The "Fresnel Array Spacecraft" will contain separate on-board opto-electronics and thrusters to carry out alignment and attitude control. It comprises transmitters, receivers, laser diodes located in the Fresnel array corners. Concerning formation flying, the "Fresnel Array Spacecraft" would be a in slave mode. The "receiver spacecraft" measurement apparatus and calculators would control the alignment, attitude, and position of the "Fresnel Array Spacecraft".

V.2.3 The “Field Optics” payload element

The “field optics” is the first payload elements encountered by light in the "receiver spacecraft". This is also the primary component concerned with chromatism correction. We propose an off axis mirror telescope as field lens, whose primary mirror only would be common to every spectral channel.

Two important parameters characterize this payload element.

– **D** : The diameter of its entrance pupil.
Its proposed value is D = 60-70 cm

– **Fs** : Its focal distance.

D determines both the observable field range and the spectral bandwidth of each channel. **Fs** is related to essential features of next payload elements in the chromatism correction trains, the blazed Fresnel lenses. Fs is expressed in V.2.3 and the formula establishing D is explained in chapter VI.

Each channel will have a dedicated focal length. To make **Fs** conform to the running channel, one might envisage a different combination of two or three optics per channel as the field optics e.g. {the common field optics primary mirror + one specific secondary mirror + one optional specific lens or mirror}. Indeed, it might be requested

that long Fs focal distance be distributed among three optical elements.

With this design, the value of **Fs** is simply selected by modifying the attitude angle of the "receiver spacecraft" with no optical element displacement. In this manner, the beam is pointed at the dedicated field optics secondary mirror and channel module, assuming that the primary mirror of the field optics has sufficient unaberrated image field. In addition, a variable focal length field optics is better, this allows to modulate the central wavelength of a spectral channel.

The field optics would also be employed as a "Super Stellar Sensor" (see VI.3.3).

V.2.4 The Blazed Fresnel Lenses

Each channel will own its proper Blazed Fresnel Lens to perform a fitted chromatism correction.

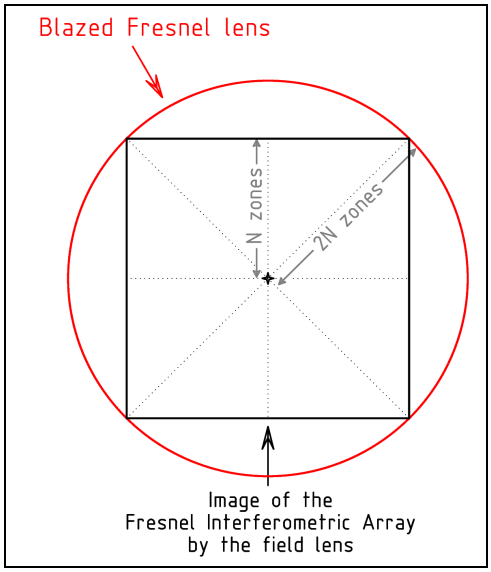

How to achieve chromatism correction. (V.4)

– **1** The Blazed Fresnel lens is located in the pupil plane i.e. at the same location as the Fresnel interferometric array image given by the field optics.

– **2** For a blazed Fresnel lens working at order –1, its number of Fresnel zones must be twice as that of the primary Fresnel array.

– **3** Each Fresnel zone image of the Fresnel array must have identical size to its corresponding Fresnel zone on the blazed Fresnel lens. **Fs** should be so adjusted to provide the correct magnification.

– **4** As illustrated here (Fig V.4), The Fresnel array image and the blazed Fresnel lens need to be superimposed and well centered. It is required that each of its Fresnel zone match its corresponding image.

Fig V-4: Chromatic correction in pupil plane

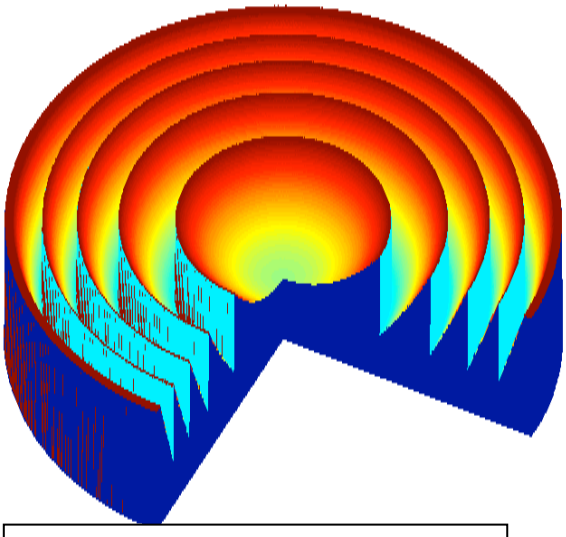

Fig V-5: 3D view of the five first Fresnel zones of an order –1 -blazed Fresnel lens.

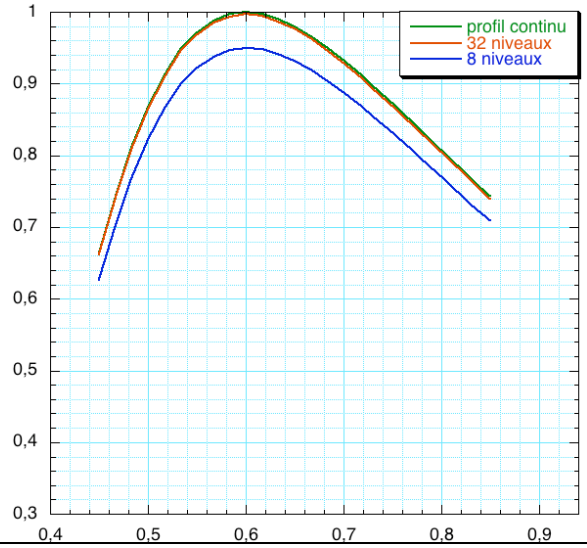

Fig V-6: Normalised efficiency of a blazed Fresnel lens at order –1 versus wavelength (in µm). The two top curves are quasi superimposed. They correspond to a non digitized blaze profile and a 32 steps blaze profile. The lens in the prototype Fresnel imager tested has 128 levels.

One can see clearly the concentric Fresnel zones in Fig V.5. A Fresnel lens works by refraction. The height transition between a zone and the next one induces an optical path difference of exactly one wavelength, if

seen from –1 order focus. The blazed profile optimizes the ratio of energy sent in –1 order focus that can attain 98 % (Fig V.6). When working in U.V, one ought to design "blazed Fresnel mirrors" that diffract light on a reflecting grating surface.

In visible range, the blazed Fresnel lens is made of fused silica. To carve the Fresnel zones, three technologies are available: chemical etching for building a continuous phase profile, ionic attack with successive masks deposit to build a quantized phase profile, and "cold" ablation provoked by a femto-second laser. At the moment, the most evolved technology we used in our prototype is the second. With a 7 masks deposit, a 2^7 = 128-level quantized surface profile is carved. The carving depth is given by : $\mathbf{H_{max} = \lambda_c / (n(\lambda_c) - 1)}$, where $\mathbf{\lambda_c}$ is the channel central wavelength and $\mathbf{n(\lambda_c)}$ the refraction index of the material at λ_c. If the blazed Fresnel lens is operated at wavelengths that goes away from λ_c , its power efficiency falls (Fig V.6) but its chromatic correction capacity remains however unimpaired.

We have to consider two pertinent parameters for the blazed Fresnel lens:

– $\mathbf{N_b}$: its number of Fresnel zones. We simply get $\mathbf{N_b = 2N}$, to satisfy condition 2 of chromatism correction principle (Fig V.4 in V.2.3).

– $\mathbf{\Phi_b}$: Its useful diameter. (equal to the outer Fresnel zone diameter). A 16 mm diameter satisfactory one has already been made for our prototype. For a 1200 to 1600 Fresnel zone lens, we expect that diameters stretching from 16 mm to 300 mm are conceivable, depending on the design wavelength and other variables.

Notice that the blazed Fresnel lens smallest zone has a width of $\mathbf{L_{min} = \Phi_b / (8\ N)}$. For example, if a suited one is built for N = 700 and $\mathbf{\Phi_b}$ = 20 mm, we get L_{min} = 3.6 µm. At present, any technological hardness is imposed by L_{min} value : Fresnel zone widths that go down to a sixth of micron are feasible. The maximum slope would be a more decisive factor. Currently, the known technical limitations are : $H_{max} / L_{min} < 1.0$ and $L_{min} > 0.2$ µm.

Let us establish an approximate relation linking $\mathbf{F_s}$, $\mathbf{\Phi_b}$, $\boldsymbol{f(\lambda_c)}$, and $\mathbf{C_{gr}}$ that complies with the second requirement of the chromatism correction (V.2.4) :

$$\mathbf{F_s \approx f(\lambda_c)\ \Phi_b / (\Phi_b + C_{gr}\ \sqrt{2}\ )}$$

V.2.5 Convergent relay optics

It should consist of a simple convergent optics that focuses the chromatically corrected image onto the camera sensor. The most important parameter here is its focal distance, $\mathbf{F_{ro}}$.

In the case of short wavelength (U.V), a different approach could be considered. Seeking a way to reduce the number of reflecting surfaces, we propose a 2-in-1 optics design that combines both the "Blazed Fresnel Lens" and "Convergent relay optics". It could consist of a concave off-axis mirror upon which is carved a "blazed Fresnel grating" that owns the same optical properties as the blazed Fresnel lens (N_b circular homothetic Fresnel zones blazed at order –1). The convergent power of the mirror overall curvature would play the focussing role of the relay optics.

VI Basic formation flying key factors

VI.1 Key system parameters

We have placed inTable VI-1 some basic key factors for the Fresnel Interferometric array imager. The parameters specific to the scientific mission (λ_{min} , λ_{max} , θ_{max} , ρ_{min} , λ_c , $\Delta\lambda$, **Q**) are in blue and those which concern particularly the distributed instruments (**Cgr** , **N** , **F** , **Ds** , **D**) are in black.

Fundamental entrance parameters		***Main implied features***	
Description	*Variable name*	*Description*	*Variable and formula*
Size of the side of the Fresnel Interferometric Array (metre)	**Cgr**	Angular resolution limit (radian)	$\rho_{min} = \lambda / Cgr$
Fresnel Number (Number of Fresnel zones)	**N**	Central wavelength for a single channel	$\lambda_c = (\lambda_{max} + \lambda_{min}) / 2$
Minimum wavelength of the imaging (metre)	λ_{min}	Wavelength span for a single channel	$\Delta\lambda = \lambda_{max} - \lambda_{min}$
Maximum wavelength of the imaging (metre)	λ_{max}	Inter-vessel distance. It corresponds to the focal length of the Fresnel array at λc (F = f(λc))	$\mathbf{F} = (Cgr)^2 / (8\ N\ \lambda c)$
Object half-field angle (radian)	θ_{max}	Required field optics minimum pupil diameter at nil object field	$\mathbf{Ds} = Cgr\ \Delta\lambda / (\lambda c\ \sqrt{2})$
Requested wavefront quality (demand ΔOPD < λ/Q)	**Q**	Field optics minimum aperture diameter required for a θ_{max} half field	$\mathbf{D} = Ds + 2\ F\ \theta_{max}$

Table VI-1: Some basic spacecraft key factors for a given spectral channel

We can distinguish two classes of parameters: the permanent ones {Cgr , N , D} that are material variables common for all missions, and the volatile ones, that can vary according to the desired scientific mission. In this way, the main implied features depend on the chosen channel: [λ_{min} ; λ_{max}] and angle from the centre of the field: θ_{max}. In this way, the inter-vessel distance ought to be adjusted accordingly to the median wavelength and the diameter of field optics, **D**, must be large enough to satisfy all channel requirements. If D(j) is the required field optics diameter of band j while there are k different spectral channels, we take obviously :

$$\mathbf{D} = \max \{D(j)\}\ \{j = 1 \ldots k\}$$

Fig VI-1 shows the field limitation entailed by the field optics. Parameter **Ds** corresponds to the field optics aperture required to collect the whole “order+1” flux in the [λmin , λmax] band, if we accept a quasi-nil field. So **Ds** is a relevant parameter for a "spectrometer mode". Parameter **D** is the minimum field optics aperture diameter required to collect all the “order+1” images in a field range [– θ_{max} ; θ_{max}]: the field in this angular range is free from vignetting.

There is a compromise between field coverage and spectral coverage at a given inter-spacecraft distance. For a given size of the field optics mirror, there is a limited domain in a two-dimensional field-waveband space where the beams are unvignetted. This full resolution domain corresponds to the plateau represented in Fig VI-2.

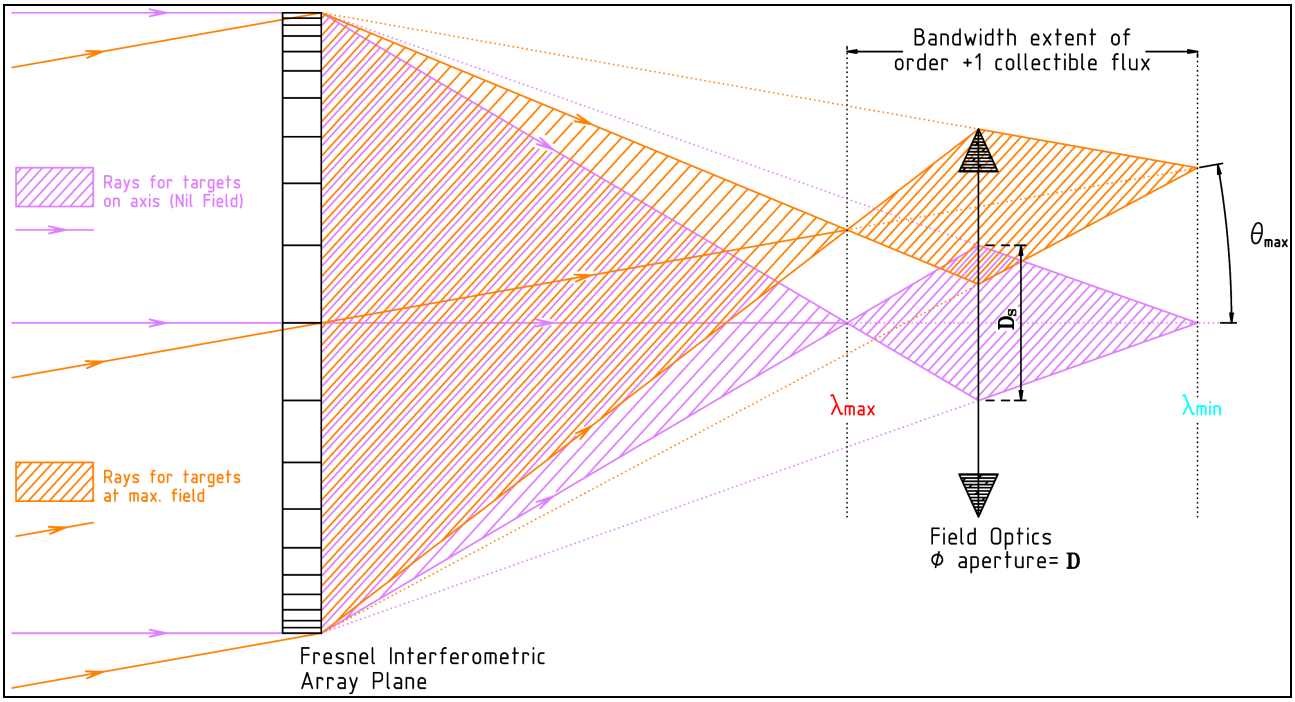

Fig VI-1: Behavior of order +1 rays versus field and unvignetted field extent.

Actually, even for the nominally unvignetted conditions, there may be wavelengths still coming from outside the interval [λ_{min}; λ_{max}]. Vignetting occurs for this external part of the spectrum due to the defocused beam at the prime focus getting larger than the field optics aperture. At these external wavelengths, both the collected flux and the angular resolution are reduced, and this a dim, low resolution PSF is added to the nominal PSF. Thus, high dynamic range imaging requires that the bandpass is actively clipped by a filter to remove the residual light outside [λ_{min}; λ_{max}]. Low dynamic range imaging and spectrometric modes should not require clipping the bandpasses.

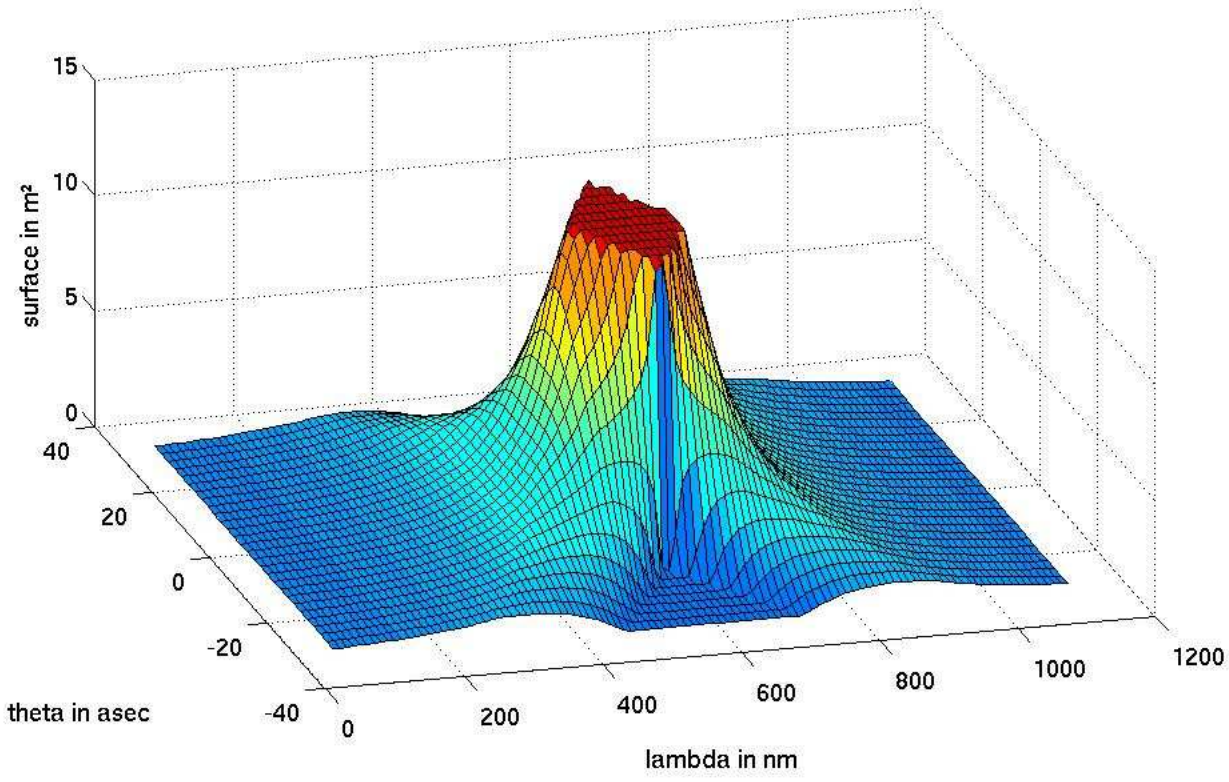

FigureVI-2: Active area of the main array as a function of the wavelength and the angle with regard to the centre of the field. The plateau corresponds to the full aperture (unvigneted), the side-lobes correspond to the decrease in beam section due to vignetting by the edges of the field optics when at off-limit wavelengtsh (lambda) or field angles (theta). This example is for the inter-spacecraft distance adjusted to a 600 nm central wavelength.

VI.2 Definition of reference frames, axes, distances and angles for the formation control.

During a pre-phase 0 study, we have established reference points (Table VI-2), reference axis (Table VI-3), reference frames and its related trihedrons (Table VI-4) for the formation and attitude control. They are depicted in Fig VI-3. Indices have the following meanings: "p" stands for "primary optics" ; "s" is related to both "secondary optics" and "short optical axis" ; "b" stands for "blazed Fresnel lens" ; "L" stands for "Long optical axis" ; "T" refers to "Target axis".

reference points	*definition*
O_p	centre of the Fresnel interferometric array foil
O_s	centre of the field optics entrance pupil
C_b	centre of (the rear) side of the blazed Fresnel lens

TableVI-2: Definition of the three reference points.

reference axis	*passes through points :*	*particularity*
"Short optical axis"	**(O_s , C_b)**	Specifies the common optical axis of the payload elements in the "receiver spacecraft"
"Long optical axis"	**(O_p , O_s)**	Connects up the two vessel centres. The Long optical axis represents the vertebral column of the Fresnel Interferometric Imager formation. All angle attitudes for servo-controlling the formation flying are set up with respect to that axis
"Target axis"	**(O_p , target center)**	Sets the formation flying direction pointed at.

Table VI-3: Definitions and particularities of the three reference axis of the formation.

Reference Frame	*Attached to :*	*Trihedron*	*Origin*	*X Y plane*	*Z direction*
"Fresnel Interferometric array reference frame" (FIA-RF)	"Fresnel Array Spacecraft"	(X_p ; Y_p ; Z_p)	**O_p**	X_p and Y_p belong to the Fresnel array plane and follow the orthogonal direction of subaperture edges.	Z_p is perpendicular to that plane and is directed toward the target.
"Receiver Spacecraft reference frame" (RS-RF)	"receiver spacecraft"	(X_s ; Y_s ; Z_s)	**O_s**	X_s and Y_s directions are aligned to the orthogonal ones of the camera sensor matrix.	Z_s is parallel to the "Short optical axis" and is directed toward the "Fresnel Array Spacecraft"
"Long Optical Axis reference frame" (LOA-RF)	"Long Optical Axis"	(X_L ; Y_L ; Z_L)	**O_p**	X_L : O_s, O_p, X_p and X_L are in the same plane. Y_L : O_s, O_p, Y_p and Y_L are in the same plane	Z_L direction is [O_s , O_p], parallel to the "Long Optical Axis"

Table VI-4: Definitions of the three orthonormal reference frames delineated by their respective trihedron.

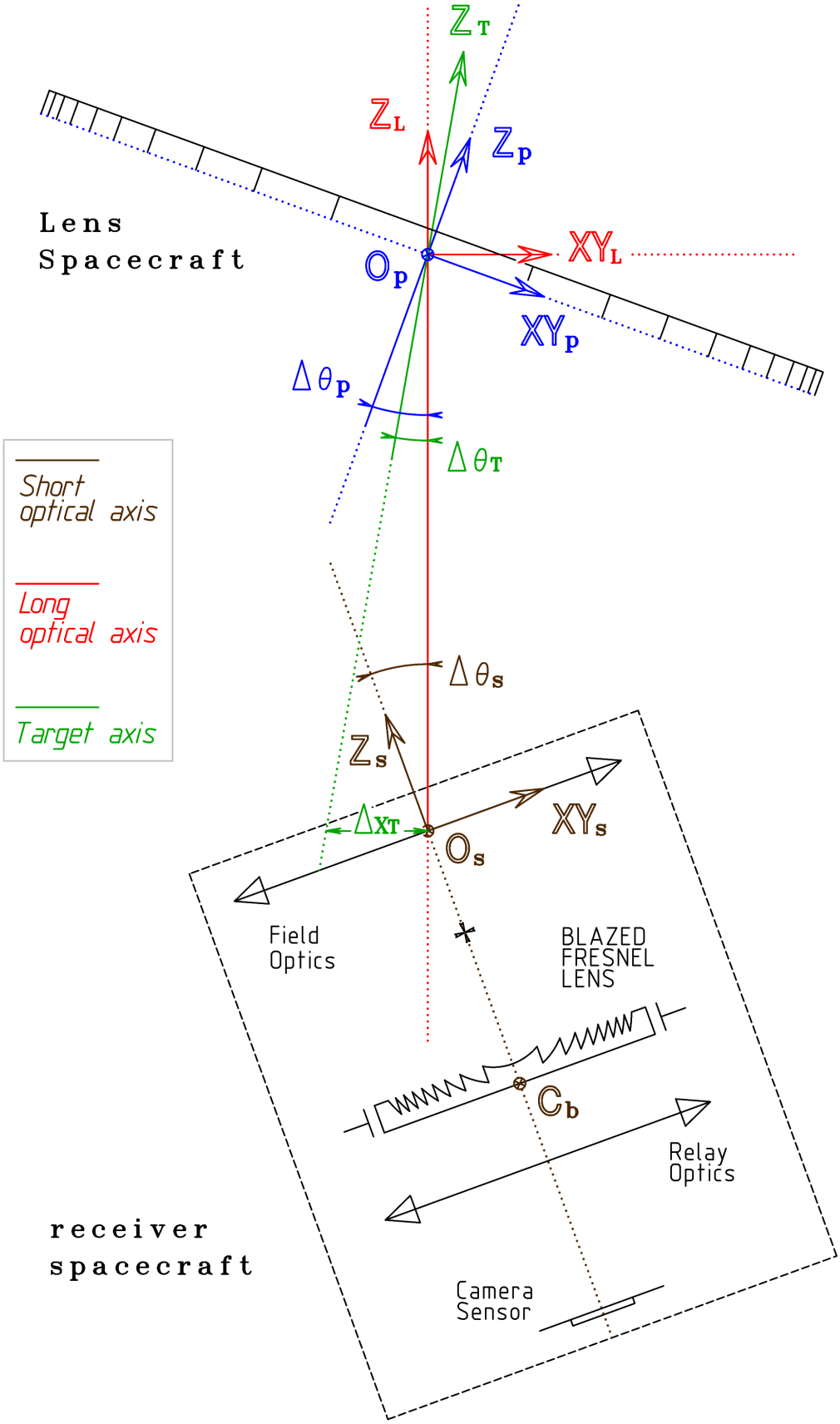

Fig VI.3: reference frames, points, angles and axis for the Fresnel Interferometric Imager.

Let us define now the three attitude angles of the Fresnel interferometric imager formation :

$\Delta\theta_T = (Z_T , Z_L)$. It is the angle between the "Target axis" and the "Long optical axis".

$\Delta\theta_s = (Z_s , Z_L)$. It is the angle between the "Short optical axis" and the "Long optical axis".

$\Delta\theta_p = (Z_T , Z_p)$. It is the angle between the "Target axis" and the vector Z_p direction.

These two first attitude angles, $\Delta\theta_T$ and $\Delta\theta_s$, are the most critical for the attitude control.

VI.3 Formation Flying Guidance Navigation & Control (GNC)

VI.3.1 Formation GNC preliminary design

We define here the distance requirements on the formation:

ΔF is the error on the inter-vessel distance. It is foremost driven by conditions 1 and 3 of chromatic correction (V.2.4). We actually must insure that the image of the Fresnel interferometric array is correctly focused in pupil plane and have the correct dimension.

Δx_T is simply deduced from the relation $\Delta x_T = F \,.\, \Delta\theta_T$. It represents the distance amount of which the "receiver spacecraft" has to be moved to compensate for the $\Delta\theta_T$ error.

Δr is specific to the Fresnel interferometric array defects (Table V-1). Not only drive they constraints on the array construction, but also demands on array warping and distortion tolerances during operation. Besides, $\Delta\theta_p$ tolerance is completely correlated to a Δr error. Consequently, the Fresnel array foil should be maintained rigid and undistorted ; in addition, temperature gradients in it should be avoided.

We give in (Table VI-5) these attitude parameters in function of basic spacecraft key parameters. Tolerances on $\Delta\theta_T$, $\Delta\theta_s$, ΔF, Δr, are expressed as stability requirements to meet during an image acquisition, which could last several hours.

Description	*Variable name*	*Requirement*
Long optical axis pointing error	$\Delta\theta_T$	$\Delta\theta_T < \lambda_c / C_{gr}$
Short optical axis pointing error	$\Delta\theta_s$	$\Delta\theta_s < \lambda_c^2 / (C_{gr}\,\Delta\lambda)$
Fresnel array pointing error	$\Delta\theta_p$	(*) $\Delta\theta_p < 1 / \sqrt{(N\,Q)}$
Inter-vessel distance error	ΔF	$\Delta F < F / (4\,N\,Q)$
Primary array warping or distortion error	Δr	$\Delta r < C_{gr} / (2\,N\,Q\,\sqrt{2})$

TableVI-5: requirements for the Fresnel interferometric imager formation attitude control.

(*) The accurate requirement for $\Delta\theta_P$ is $\Delta\theta_p < \frac{1}{NQC_{gr}}\sqrt{8N^4\lambda^2Q^2 + NQC_{gr}^2} - \frac{2N\lambda\sqrt{2}}{C_{gr}}$

For short wavelength (U.V), a rough approximation is given by: $\Delta\theta_p < \frac{1}{\sqrt{NQ}}$. One can show that its value is relatively relaxed. This is caused by the intrinsic properties of Fresnel interferometric array foils that have released tolerances (Table V-1)

Before acute attitude control, we may proceed to the initial alignment and tracking of the target. To put an astrophysical object in the field of view of the field optics, the condition on $\Delta\theta_T$ during initial alignment is

$\Delta\theta_T$ (a) < $D_s / (4\,F)$

Then, this target order +1 image demands to be correctly centered in the field optics, just before the image acquisition phase. We get here an initial tracking condition on $\Delta\theta_s$, driven by the necessity of centering the target in field of the "Super Stellar Sensor" :

$\Delta\theta_s$ (c) < $45\,C_{gr} / (F\,N)$ in U.V range and $\Delta\theta_s$ (c) < $22\,C_{gr} / (F\,N)$ in I.R range.

Let us describe the way of proceeding to achieve the formation control, in six steps:

– We first align the "Target axis" onto the "Long optical axis". The Super Stellar Sensors determine the corresponding $\Delta\theta_T$ pointing error (seeVI.3.3), which equals the angular distance between point O_P and the punctual target as seen from point O_s. The $\Delta\theta_T$ angle should be so led back to nil by translating the "receiver spacecraft" of the above $\Delta x_T = F \,.\, \Delta\theta_T$.

– Secondly, we align the "short optical axis" onto the "long optical axis". The "receiver spacecraft" would so

undergo a rotation, in order to minimize the $\Delta\theta_s$ angle.

– Thirdly, we align the perpendicular axis to the Fresnel interferometric array (O_p , Z_p) onto the "Long optical axis", so as to minimize $\Delta\theta_p$. Only a very gross actuation is needed here because of the released tolerance on $\Delta\theta_p$.

– Next, a rotation of the "Fresnel Array Spacecraft" around the "Long optical axis" is certainly necessary, to orient the orthogonal spikes of the Fresnel interferometric array PSF into the wanted direction.

– Then, a rotation of the "receiver spacecraft" around the "short optical axis" is expected. We actually need to make Xs and Ys parallel to the Fresnel array axis Xp and Yp, in the purpose of superposing the sensor matrix axis with the two spikes of the said PSF.

– Finally, a longitudinal translation of the "receiver spacecraft" would be processed e.g. along the "long optical axis" with the aim of canceling the inter-vessel distance error, ΔF.

VI.3.2 Formation GNC preliminary requirements

Fundamental input parameters	Band 1 (UV)		Band 2 (UV)		Band 3 (UV)		Band 4 (UV)		Band 5 (Blue)		Band 6 (IR)	
Fresnel number (N)	700											
Wavefront Quality (Q)	25											
Size of square array (Cgr) (in m)	3,6											
mode : spectro --> broad spectral bands, narrow field ; imager --> vice versa	imager	spectro	imager	spectro	imager	spectro	imager	spectro	imager	spectro	imager	spectro
Minimum wavelength (µm)	0,123	0,110	0,160	0,143	0,208	0,186	0,270	0,241	0,387	0,345	0,895	0,800
Maximum wavelength (µm)	0,130	0,143	0,169	0,186	0,219	0,241	0,284	0,313	0,408	0,448	0,940	1,035
Half field angle (arc second)	3,12	0,09	4,05	0,11	5,26	0,23	6,82	0,23	9,77	0,33	22,60	1,14
Main implied features												
Central wavelength (µm)	0,127		0,165		0,214		0,277		0,397		0,918	
Wavelength span (µm)	0,006	0,033	0,008	0,043	0,011	0,055	0,014	0,072	0,020	0,103	0,046	0,235
Relative spectral band	0,05	0,26	0,05	0,26	0,05	0,26	0,05	0,26	0,05	0,26	0,05	0,26
Angular resolution limit at central wavelength (mas)	7,25		9,43		12,23		15,87		22,72		52,57	
Inter-vessel distance (m)	18 295		14 069		10 840		8 355		5 837		2 522	
Required field optics aperture at nil field (Ds) (in m)	0,13	0,66	0,13	0,67	0,13	0,66	0,13	0,66	0,13	0,66	0,13	0,65
Number of linear resolution elements in unvignetted field (resel)	860	25	860	23	860	38	860	29	860	29	860	44
Required diameter of Field optics for global mission (m)	0,68											
Tolerances for attitute control												
Long optical axis pointing error (mas)	7,2		9,4		12,2		15,9		22,7		52,6	
Short optical axis pointing error (mas)	145,0	27,8	188,5	36,1	244,7	47,5	317,4	61,1	454,4	87,5	1051,4	205,2
Fresnel array pointing error (degree)	0,43		0,43		0,43		0,42		0,42		0,41	
Inter-vessel distance error (mm)	261,4		201,0		154,9		119,4		83,4		36,0	
Fresnel array warping or distortion error (µm)	72,7											

Table VI-6: Proposed numerical values for The Fresnel Interferometric Imager main parameters.

In Table VI-6 are presented the essential numerical values for the proposed class L Fresnel Interferometric Imager. For each channel, we consider two simultaneous operating modes. The "imager mode" is characterized by a narrow relative spectral band (0.05 – 0.02) but also by the maximum available objet field. In the other hand, the "spectrometer mode" gets the widest relative spectral band (0.26) and a relatively tiny objet field. This "spectro mode" is dedicated to recover the spectrum of astrophysical objects laid in the central pixels of the field.

In order to have both a broad field image and the possibility of spectral range, we propose the simultaneous use of an imager and a spectrometer, the entrance "slit" of the spectrometer taking out the central pixels of the field.

The bandwidths indicated here are conservative: they suppose a zero vignetting situation. It is possible to increase the field or the spectral coverage, the PSF will slowly degrade as the field increases.
Waveband choice and causes of waveband limitation:

Once launched, the six bands will not be changed, and if they do not overlap there will be gaps between them in the spectral coverage of the instrument. Here is an example of possible spectral coverage, with four bands in the UV and two at larger wavelengths:

λ (µm)	0.120	0.180	0.280	0.500	0.730	1.000
Δλ/λ	0.27	0.27	0.27	0.27	0.27	0.27
Δλ	3.21E-8	4.67E-8	7.48E-8	1.34 E-7	1.94E-7	4,71E-7
λmin	0.104	0.152	0.243	0.434	0.631	0.866
λmax	0.136	0.198	0.317	0.568	0.825	1.134

Table VI-7: Example of possible wavelengths channels obtained with a 68 cm field mirror and a 600 zone, 3.6x3.6 Fresnel array.

Observing at full angular resolution outside these predefined spectral bands will be possible, but with lower performances in dynamic range and at the cost of more complicated focal optics.

Full aperture and angular resolution can be reached at an arbitrary wavelength by adapting the inter-spacecraft distance, but this change in distance will cause the chromatic dispersion corrector lens to be "out of focus" for the resulting pupil plane, and furthermore, the size of the pupil will no longer be equal to the size of the correcting lens. Residual chromatism will appear. This can be solved by having an additional optical element (lens or mirror) in the corresponding optical train that can be shifted a few millimetres into position, this allowing a shift of the full-aperture corrected waveband, but this configuration has not been studied nor tested yet.

For a shifted waveband, far from the central wavelength adapted to the blaze angle of the chromatic corrector, the dynamic range will be limited by the leak in this blazed correcting Fresnel lens from order+1 into other diffraction order, ending up as stray light in the field. The tolerance in waveband can be seen in fig. V-6.

In each of the six channels, the chromatic dispersion corrector lens is blazed for maximum efficiency at a predefined wavelength. The performance degradation is in dynamic range : even though it has is a better than 75% efficiency in a band $\Delta\lambda/\lambda = 0.4$, part of light that is not transmitted ends up as diffuse illumination and reduces the dynamic range. This is not important for normal imaging but crucial for very high dynamic range applications like exoplanet study. The simulation of blazed Fresnel lens efficiency in Fig V.6 is the demonstration of that phenomenon.

To put it in a nutshell, the higher the rejection rate requested, the closer we must be to the central blazed wavelengths of each channel.

VI.3.3 Formation Flying fine navigation (super stellar sensor)

We propose to use the receiver field optics "telescope" as a super fine stellar and lateral sensor, fed by the zero order of the primary array. Both the background stellar reference(s) and the fiducial light patterns on the primary array will be imaged on a dedicated detector. The angular separation $\Delta\theta_T$ between the stellar reference and the long optical axis [Os-Op], can be measured this way.

The angular separation $\Delta\theta_S$ between the field optics telescope optical axis and the long optical axis can be measured by the relative image position of the fiducial light patterns with regard to references internal to this super stellar sensor.

VI.4 Mass, resources and Thrusters :

In Table VI-8, the masses of the different units composing the formation are estimated.

Element	***Mass (kg)***
"Fresnel Array Spacecraft" platform	400
Fresnel Interferometric Array (structure + baffle + basic deployments)	200
Adaptor & SYLDA-Soyuz	300
"receiver spacecraft" platform	500
Payload units of "receiver spacecraft"	500
Grand TOTAL	**1900**

Table VI-8: estimated unit masses

In case of tight mass limits for the launching capacity of Soyuz to L2 (nominally 2000 kg), the secondary spacecraft mass can be reduced at the price of reducing the number of spectral channels.

Achieving the attitude control :

Both spacecrafts would be equipped with **cold gas propulsion** for fine lateral and longitudinal control during operations. These would besides enable **reaction wheel** off-loading: for precise attitude control, we suggest reaction wheels for both spacecrafts**.**

If this proposal is accepted, we propose to study **solar sail** attitude control, on the "Fresnel Array Spacecraft" shipboard.

The two spacecrafts would be equipped with **Hall-Effect Plasma Thrusters.** They would manoeuvre the spacecrafts with gross actuations : First, they would be involved in orbit corrections for final orbit injection around L2. Second, they would be employed to modify the inter-vessel distance, to change the target pointing and to perform station keeping during the mission lifespan. We propose **PPS-1350**, same as those which already equip Smart-1. Their known specific impulse approaches 1500 s and their thrust reach the range (30 mN – 80 mN). As they require electrical power from 0.46 to 1.2 kW, each spacecraft will need 2 kW solar cells, which correspond to a 10 – 14 m^2 surface.

The spectrum scanning implies that the spacecrafts shift back and forth toward each other. Scanning the spectrum from U.V to I.R in the six channels requires that the "receiver spacecraft" stop at each intermediate distance mentioned in Table VI-6. The formation must be still when observing on every channel to keep the attitude control. In this way, ten accelerations or decelerations per target are needed to cover the spectrum.

A raw estimation of gas mass can be done : assuming an acceleration ΔV = 0.5 m/s , and a 1000 kg weight spacecraft, a gas mass of 0.33 kg per target is necessary.

VII Science Operations and Archiving

In order to save propulsion reserves and mission duration, the observing runs will have to be optimized in terms of wavelength shift and pointing direction. The baffles allowing a +/- 20 degrees pointing latitude with regard to the plane perpendicular to the Sun direction, a complete sky coverage is possible in less than 6 months.

During the lifetime of the mission, we project to observe 1000 target objects with a mean time per target of 40 hours, each target being observed sequentially at various wavelength channels. The inter-spacecraft distance will be stabilized and adapted for each band during integration of images and spectra (possibly simultaneous). Some targets will be observed with integrations times as long as 100 hours, others will require less than 1 hour. The dead time between integrations due to target shift and / or waveband shift is estimated at 20% of the total observing time. During one single travel along the optical axis, corresponding to a scan of the global observable spectrum, a given astrophysical target can be observed in the six spectral bands. Two targets can be fully imaged per round-trip.

The light feeding the spectrometric equipment will not contribute to the image, thus creating a small “blind spot” a few pixels wide in the image, representing the entrance slit or fibre of the spectro. An additional way to obtain spectral data, without using the internal dispersion equipment of a channel, is to make a rotation of a few arc minutes of the receiver spacecraft (field telescope optical axis), which would induce linear dispersion in the final image fields, thus providing low spectral resolution dispersed broad field.

The image and spectral data storage requirement will be in the order of 4 megabytes per image or per spectrum, at a maximum rate of a few images and spectra per hour : a maximum data rate of 20 megabytes per hour, approximately 50 kilobits per second.

Proprietary data policy : Conformally to the ESA guidelines, the data will be publicly available immediately or after a three months delay.

VIII Key technology areas

The different "Technology Readiness Levels" of technologies and payload units involved in the Fresnel Interferometric Imager are given in table VIII-1.

Payload unit /Technology	***Current developments***	***TRL level***	***Improvements to be scheduled***
Fresnel interferometric array	A 58 Fresnel zone-array of 80 mm square size has been tested. It was carved by a UV laser in an 80µm steel foil, comprising 26 680 rectangles.	**04**	Design and test of subaperture patterns and apodization functions that improve the dynamic range. Industrial processes that enable carving large metal foil, typically 3.6 meters. Studies on deployment issues for future generation Fresnel interferometric arrays (e.g. 30m).
Field Optics	Maksutov-Cassegrain Skywatcher mirror telescope as the field lens. D = 150 mm, Fs = 1800 mm, visible range. Such mirrors should be ready to operate in space.	**07**	Off-axis mirror design that covers a broadband reflectivity domain. Foresee bands both in U.V (110nm), visible and at I.R (8µm).
Blazed Fresnel Lenses for U.V and I.R	Currently surveyed.	**03**	Foresee "blazed Fresnel mirror" that acts by reflexion. Fresnel zones would be carved as a grating mirror, in particular to enable working in deep U.V.
Blazed Fresnel Lens in Visible band.	A 116 zone- 16 mm- silica blazed Fresnel lens has been custom designed and built. Its blaze wavelength is λc = 600 nm.	**04**	
Chromatism correction of Primary Fresnel array images	The chromatism correction principle was corroborated during R&T 2005-2007 action. A broadband chromatism correction was achieved around 600 nm.	**04**	Assess this technology on vacuum environment with effective formation-flying constraints (can de done at ground facilities)
Whole Fresnel Interferometric Imager	Breadboard in laboratory environment (CESR white room, Toulouse, France). This breadboard operates on artificial targets, is diffraction limited and has a proven dynamic range of 6.10^{-6}	**04**	Test a model of Fresnel Interferometric Imager in a relevant environment. Point real astrophysical targets and prove its imaging capabilities on sky.
Formation-flying control	Theoretical studies. SIMBOL-X is already a 20-30 m formation flying spacecraft. R&T would extend it to 150 km.	**03**	Maintaining rigid and unwarped very large Fresnel Interferometric arrays. Controling and stabilizing the formation across huge distances (> 1000 m).

Table VIII-1: TRL levels of the Fresnel interferometric imager payload units and technologies.

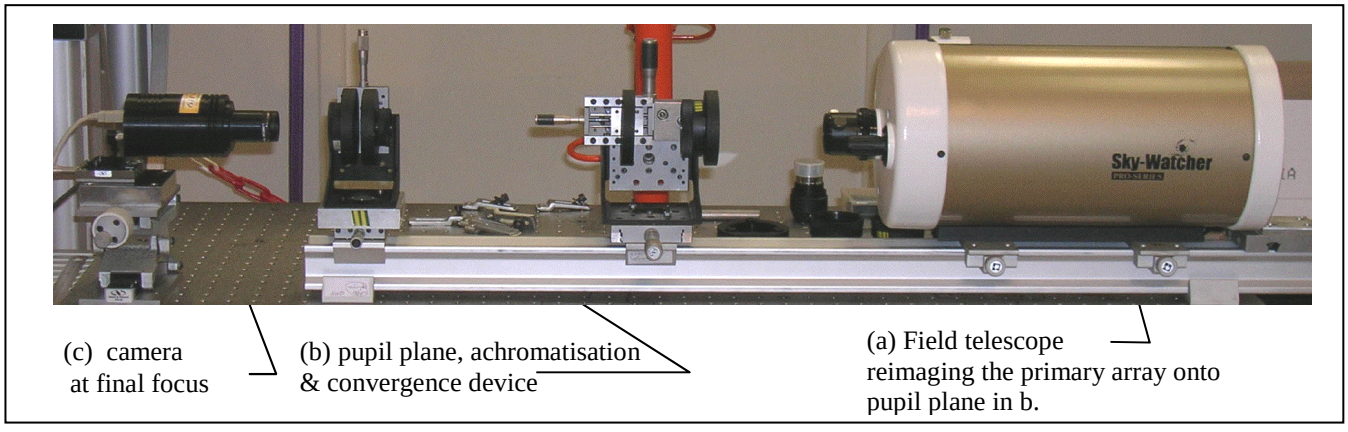

Fig VIII.1 : Field optics and focal instrumentation module of the 22m focal length prototype built at Observatoire Midi Pyrénées, to validate the Fresnel Interferometric Imager concept. The 80 mm, 26680 aperture prototype Fresnel array is placed at a 22 metre optical path upstream. It is displayed in fig.1.3 at the beginning of this document. The field telescope used here is diaphragmed to a diameter of 20 mm and used off axis. The chromatic corrector is a custom designed fused silica diffractive lens, 20 mm in diameter with 116 cophased Fresnel zones, blazed for a wavelength of 600 nm. The tests on artificial sources made with this prototype prove the broad band diffraction limited imaging and high dynamic range capabilities of the concept (6 10^{-6} at present, without the future coronagraphic module).

The primary Fresnel interferometric array module (Fig I.3) is an 80 mm square, 58 Fresnel zones (26,680 subapertures) grid carved into an 80 μm metal foil.

The focal instrumentation module (Fig VIII.1) comprises a field telescope (a), which re-images the primary array onto a fused silica diffractive blazed lens (b) placed at a pupil plane. A CCD camera (c) captures the images at the final image plane. We are also working on a coronagraphic design, which should also improve the dynamic range.

IX Preliminary programmatics / Costs

The mission should be achievable within the cost and time constraints of an L type mission. The distribution of costs would conform to that of Table 5b given in Annex 4 of the Cosmic Vision Call.

The secondary optics should fit on a standard satellite platform. We expect that the "receiver spacecraft" to consume the greater part of the "Total spacecraft industrial activities".

More detail would be given at the end of the Phase 0 study recently opened by the French Spatial Agency C.N.E.S. [09].

Payload / Spacecraft unit	***Costs (Millions euros 2007)***
"Fresnel array Spacecraft"	
Platform unit (comprising telemetry, power units ...)	75
Margin on platform unit (20%)	15
All Payload elements with margin	60
Middle total	150
Contingency on "Fresnel array Satellite"(10%)	15
System Studies	8
GRAND TOTAL for the "Fresnel array Spacecraft"	**173**
"Receiver Spacecraft"	
Platform unit (comprising telemetry, power units ...)	100
Margin on platform unit (20%)	20
All Payload elements with margin	100
Middle total	220
Contingency on "Receiver Spacecraft"(10%)	22
System Studies	11
GRAND TOTAL for the "Receiver Spacecraft"	**253**
Soyuz Launcher and launch services	55
Ground Segment	60
TOTAL Fresnel Interferometric Imager Formation	**541**
Pre-Implementation Phase (1%)	5
ESA Internal Costs (11%)	60
GRAND TOTAL for the 10 year-mission	**606**

Table IX-1: Estimation of overall costs for the proposed mission

Assumed share of payload costs to ESA:
1. The whole "Fresnel array Spacecraft" with its Fresnel Interferometric Array.
2. The whole field optics {the primary mirror + the six secondary mirrors + standard optics}
3. The Blazed Fresnel Lenses and relay optics.

X Communications and Outreach

The collaboration has just started between astrophysicists groups in France, Spain and the Center for Astrophysics in the U.S.A., The respective role and share of all is not defined yet, as discussions are taking place with other scientists who plan to join us in the near future.

XI Bibliography

[01] L. Schupmann, "Die Medial Fernrohre : Eine neue Konstruktion for grosse astronomisch Instrumente" (B.G Teubner, Leipzig, 1899)

[02] R. A. Hyde, "Eyeglass : Very Large Aperture Diffractive Telescopes" Applied Optics 38, No. 19, 4198-4212, (1 July 1999).

[03] L.Koechlin, J-P. Perez : "A limit in Field-resolution ratio for interferometric arrays", Wesley A. Traub, Editor **SPIE** Proc Vol. 4838 411-415, "Interferometry for optical astronomy, II" Hawaii, août 2002.

[04] L. Koechlin, D. Serre, P. Duchon "High resolution imaging with Fresnel interferometric arrays : suitability for exoplanet detection", Astronomy & Astrophysics vol. 443, 709-720 (2005).

[05] Yuri M. Chesnokov,"A Space-Based Very-High Resolution Telescope", Russian Space Bulletin, 1993, vol. 1 No. 2.

[06] J.T. Early "Solar sail – Fresnel zone plate lens for a large aperture based telescope", AIAA 1705, 3773-3778 (2002).

[07] D. Massonnet, brevet C. N. E. S. : "Un nouveau type de télescope spatial", Ref. 03.13403 (2003).

[08] Dean Faklis & G. Michael Morris, "Broadband imaging with holographic lenses ", Optical Engineering, Vol. 28 No.6, p 592-598 (June 1989).

[09] Phase 0 study on the "Fresnel Interferometric Imager" at C.N.E.S, Toulouse, France. Emmanuel Hinglais is responsible for this study starting now (The pre-phase 0 occurred during the 2007 first semester)

[10] H.W. Moos et al., Overview of the Far Ultraviolet Spectroscopic Explorer Mission, Astrophys. J. Letters, 538, L1-L6, 2000

[11] K.R. Sembach et al., The Deuterium-to-Hydrogen ratio in a low-metallicity cloud falling onto the Milky Way, Astrophys. J., Suppl. Ser., 150, 387-415, 2004.

[12] N. Lehner et al., Far Ultraviolet Spectroscopic Explorer Survey of the Local Interstellar Medium within 200 Parsecs, Astrophys. J., 595, 858-879, 2003

[13] G. Hebrard, H.W. Moos, The Deuterium-to-Oxygen Ratio in the Interstellar Medium, Astrophys. J., 599, 297-311, 2003

[14] G. Hebrard et al., FUSE Determination of a Low Deuterium Abundance along an Extended Sight Line in the Galactic Disk, Astrophys. J., 635, 1136-1150, 2005

D. Charbonneau et al., Detection of an extrasolar planet atmosphere, Astrophys. J., 568, 377-384, 2002
[15] A. Vidal--Madjar et al., An extended upper atmosphere around the extrasolar planet HD209458b, Nature, 422, 143-146, 2003

[16] A. Vidal--Madjar et al., Detection of Oxygen and Carbon in the hydrodynamically escaping atmosphere of the extrasolar planet HD209458b, Astrophys. J. Letters, 604, L69-L72, 2004

[17] A. Lecavelier des Etangs, A. Vidal--Madjar, J.C. McConnell, G. Hebrard, Atmospheric escape from hot Jupiters, Astron. Astrophys., 418, L1-L4, 2004

[18] D. Ehrenreich et al., The transmission spectrum of Earth-size transiting planets, Astron. Astrophys., 448, 379-393 , 2006

[19] L.J. Richardson et al., A Spitzer infrared radius for the transiting extrasolar planet HD209458b,

Astrophys. J., 649, 1043-1047, 2006

[20] G.E. Ballester, D.K. Sing, F. Herbert, The signature of hot hydrogen in the atmosphere of the extrasolar planet HD 209458b, Nature, 445, 511-514, 2007

[21] A large UV-optical telescope for characterization of the atmospheres of extrasolar planets and satellites, 39TH ESLAB Symposium on Trends in Space Science and Cosmic Vision 2020, held 19-21 April 2005, Noordwijk, The Netherlands. Edited by F. Favata, J. Sanz-Forcada, A. Giménez, and B. Battrick. ESA SP-588. European Space Agency, 73L, 2005

[22] D. Deming et al., Infrared radiation from an extrasolar planet, Nature, 434, 740-743, 2005

[23] D. Charbonneau et al., Detection of thermal emission from an extrasolar planet, Astrophys. J., 626, 523-529, 2005

[24] D.L. Richardson et al., A spectrum of an extrasolar planet, Nature, 445, 892-895, 2007

[25] C.J. Grillmair, et al., A Spitzer spectrum of the exoplanet HD189733b, Astrophys. J., 658, L115-L118, 2007

[26] H.A. Knutson et al., A map of the day-night contrast of the extrasolar planet HD189733b, Nature, 447, 183-186, 2007

[27] Karovska, M., Schlegel, E., Hack, W., Raymond, J. C., & Wood, B. E. 2005, ApJ, 623, L137

[28] Karovska, M., Hack, W., Raymond, J., & Guinan, E. 1997, ApJ, 482, L175 Chugai, N.N., and Yungelson, L.R., 2004, Astron. Lett., 30, 65.

[29] Aikawa & Herbst, 1999; A&A, 351, 233

[30] Aikawa & Herbst 2001; A&A, 371, 1107

[31] Gomez de Castro et al 2006; ApSS, 303, 33

[32] Herczeg et al 2004; ApJ, 607, 369

[33] van Dishoeck et al 2006; Faraday Discussions, 133, 231